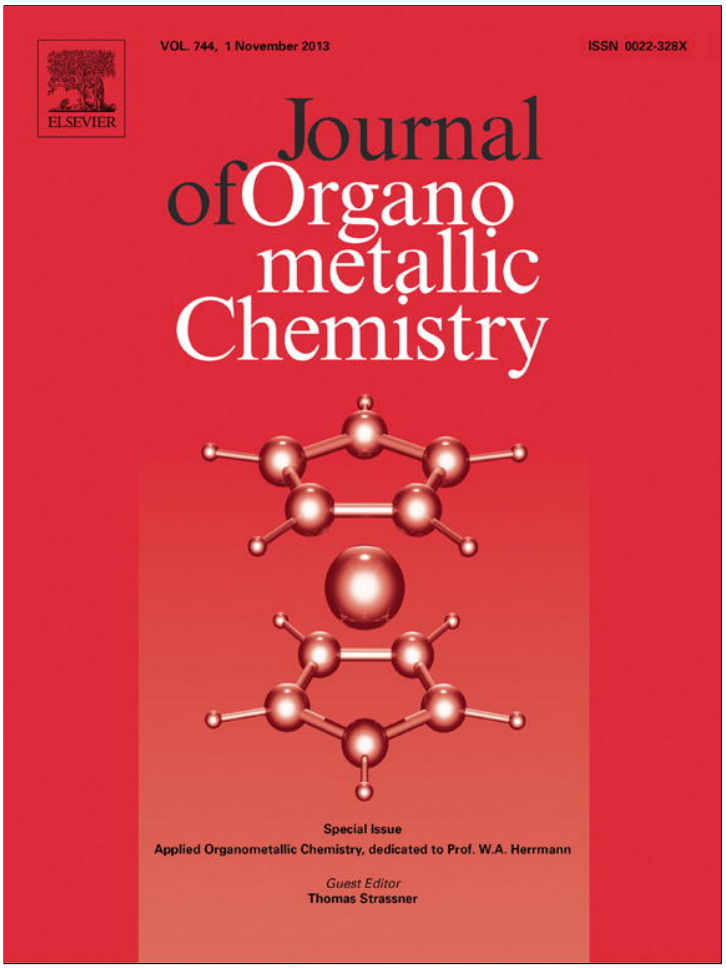

Journal of Organometallic Chemistry 744 (2013) 125–139

Contents lists available at SciVerse ScienceDirect

Journal of Organometallic Chemistry

journal homepage: www.elsevier.com/locate/jorganchem

Target-specific $Tc(CO)_3$-complexes for *in vivo* imaging

Maurício Morais, António Paulo, Lurdes Gano, Isabel Santos, João D.G. Correia*

Unidade de Ciências Químicas e Radiofarmacêuticas, IST/ITN, Instituto Superior Técnico, Universidade Técnica de Lisboa, Estrada Nacional 10, 2686-953 Sacavém, Portugal

ARTICLE INFO

Article history:
Received 8 May 2013
Received in revised form
29 May 2013
Accepted 31 May 2013

Dedicated to Prof. W.A. Herrmann on the occasion of his 65th birthday.

Keywords:
Radiopharmaceuticals
Rhenium
Technetium-99m
Pyrazolyl-containing ligands
Targeting
Biomolecules

ABSTRACT

In recent years, the remarkable characteristics of the organometallic precursor *fac*-$[M(CO)_3(H_2O)_3]^+$ (M = Re, Tc) introduced by Alberto and co-workers brought renewed interest to the development of low-oxidation ^{99m}Tc-based radioactive probes. Considering our interest in the design of target-specific radioactive probes for SPECT-imaging and targeted systemic radiotherapy, we have been involved in the study of the chemistry of *fac*-$[M(CO)_3]^+$ (M = Re, Tc) with chelators combining a pyrazolyl unit with aliphatic amines and/or carboxylic acids or thioethers. This review describes our research efforts in the field, giving particular emphasis to the biological properties of Re(I) and ^{99m}Tc(I) complexes anchored by those type of chelators. We aim to highlight the versatility of the pyrazolyl-containing chelators, which allowed the successful labeling of a wide range of relevant biomolecules, spanning from small lipophilic organic molecules, such as quinazoline derivatives or DNA-binders, to tumor-seeking peptides for *in vivo* receptor targeting. Noteworthy is also the possibility of labeling polymeric nanoparticles based on dextran for sentinel lymph node detection (SLND), which has been one of our most successful achievements in recent years. These radiolabeled nanoparticles allowed the visualization of the SLN accurately at the preclinical level.

1. Introduction

Radiopharmaceuticals are drugs that incorporate a radionuclide in their composition and are administrated to patients for diagnosis or treatment of diseases [1]. The radiotracers containing gamma(γ)- or positron(β^+)-emitting radionuclides are suitable for single photon emission tomography-imaging (SPECT-imaging) or positron emission tomography-imaging (PET), respectively, whereas those containing β^-- or α-emitters are useful for systemic radiotherapy [1–6]. The radiopharmaceuticals currently used in nuclear medicine for SPECT-imaging are mainly metal-based compounds, with technetium-99m (^{99m}Tc) accounting for the majority of the complexes used. Indeed, ^{99m}Tc is still the most important radionuclide in nuclear medicine due to its ideal nuclear properties ($t_{1/2}$ = 6.02 h; $E_{\gamma max}$ = 140 keV), low-cost, and convenient availability from commercial ^{99}Mo/^{99m}Tc generators [5]. Another relevant characteristic of ^{99m}Tc relates with its diverse and rich redox chemistry [7–10]. Among all oxidation states of technetium (-I to VII), ^{99m}Tc(V) has been the most studied and applied in radiopharmaceutical chemistry [7–10]. Although most of the ^{99m}Tc(V)-based radiopharmaceuticals in clinical use contain the core $[^{99m}Tc(O)]^{3+}$ (e.g. ^{99m}Tc-HMPAO – Ceretec®; ^{99m}Tc-MAG_3 – TechneScan MAG_3®), there is a single example of a radiopharmaceutical corresponding to a complex with the core *trans*-$[^{99m}Tc(O)_2]^+$ (^{99m}Tc-Tetrofosmin – Myoview®) (Fig. 1) [1,11,12]. Additionally, several compounds containing the cores $[^{99m}Tc(N)]^{2+}$ and [^{99m}Tc-HYNIC] (HYNIC = 6-hydrazinonicotinic acid) have been also explored both at the preclinical and early clinical level [7–10,13]. Until recently, the low oxidation states of ^{99m}Tc have received less attention than the oxidation state V, in spite of the clinical and commercial success of the organometallic complex $[^{99m}Tc(CNCH_2C(CH_3)_2OCH_3)_6]^+$ (Sestamibi) (Fig. 1) [11]. The latter, marketed under the trademark Cardiolite®, is a lipophilic cation of Tc(I) stabilized by six isonitrile ligands. Sestamibi was originally developed as a SPECT myocardial imaging agent, but nowadays is also used for both early cancer detection and non-invasive monitoring of the tumor Multidrug Resistance (MDR) transport function [14]. This complex is considered the unique organometallic pharmaceutical used routinely in medicine and, together with cisplatin, are the most successful synthetic metal complexes for medical application [11,15]. The pharmacokinetic profile of radiopharmaceuticals, and particularly of those based on ^{99m}Tc, is determined either by their physicochemical properties – *perfusion agents* – or by a combination of physicochemical features and biological interactions – *target-specific radiopharmaceuticals.* Whereas in the former the biological distribution is determined by blood flow, in

* Corresponding author. Tel.: +351 21 994 62 33.
E-mail address: jgalamba@itn.pt (J.D.G. Correia).

0022-328X/$ – see front matter © 2013 Elsevier B.V. All rights reserved.
http://dx.doi.org/10.1016/j.jorganchem.2013.05.050

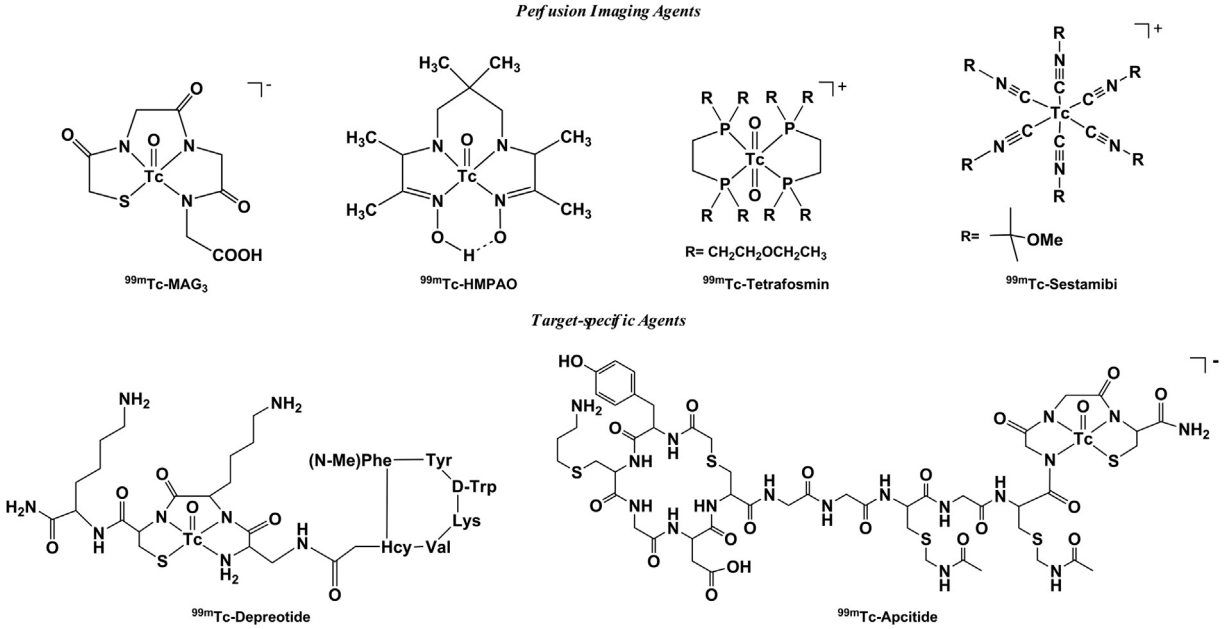

Fig. 1. Perfusion and target-specific ^{99m}Tc-based radiopharmaceuticals for SPECT-imaging.

the latter the biodistribution is also dependent on specific ligand–target interactions. The targeting ability depends on the presence of pendant biologically active molecules ("biomolecule") that recognize the respective macromolecular target. In this way, it is possible to image biochemical processes that occur at the molecular/cellular level before morphological changes occur [16–18]. A great variety of biomolecules based on monoclonal antibodies, peptides, non-peptidic small molecules, and oligonucleotide analogs, among others, have been explored for target-specific delivery of radionuclides [1,19–21]. They recognize cell markers or receptors over-expressed on malignant cells, intracellular metabolic pathways that are up-regulated in cancer or cellular processes closer to transcription. So far, among all possible approaches for the design of target-specific radiopharmaceuticals, the use of bifunctional chelators (BFCs) for linking the radionuclide to the biomolecule has been the most successful. In the case of ^{99m}Tc, we may refer ^{99m}Tc-depreotide (NeoSpect®) and ^{99m}Tc-Apcitide (Acutec®), which contain pendant cyclic peptides, and are target-specific radiopharmaceuticals approved for imaging lung tumors and acute venous thrombosis, respectively (Fig. 1).

The notable work of Alberto and co-workers led to the introduction of the organometallic species *fac*-$[M(CO)_3(H_2O)_3]^+$ (M = Re, Tc), an excellent precursor to enter into the chemistry of M(I), which brought renewed interest to the design of radiopharmaceuticals based on low-oxidation states [22–31] as alternative to classical strategies based on the cores $[^{99m}Tc(O)]^{3+}$, trans-$[^{99m}TcO_2]^+$, $[^{99m}Tc(N)]^{2+}$ or [^{99m}Tc-HYNIC].

The synthesis of Tc and Re complexes relevant for nuclear imaging (^{99m}Tc) or radionuclide therapy ($^{186/188}$Re) must be performed in aqueous solution, starting from the respective permetallates ($Na[MO_4]$) obtained by elution of the commercially available ^{99}Mo/^{99m}Tc and ^{188}W/^{188}Re generators. As regards to *fac*-$[^{99m}Tc(CO)_3(H_2O)_3]^+$, it has been firstly shown that this precursor could be obtained by treating $Na[^{99m}TcO_4]$ with $NaBH_4$ in the presence of CO in aqueous solution. However, CO is a toxic gas, unsuitable for use in hospitals and in commercial radiopharmaceutical kits, a problem which was overcome by the use of boranocarbonate, $K_2[H_3BCO_2]$. This compound reduces Tc(VII) and acts as a CO source, through mechanisms not yet fully understood (Scheme 1). The synthesis of *fac*-$[^{188}Re(CO)_3(H_2O)_3]^+$ is only possible by reducing $[^{188}ReO_4]^-$ with a combination of $K_2[H_3BCO_2]$ and amine borane ($BH_3{\cdot}NH_3$), reflecting the different redox chemistry of Tc and Re (Scheme 1).

The diluted nature of the solutions of ^{99m}Tc complexes (10^{-8} M–10^{-10} M) makes their structural characterization impossible by the current analytical methods (*e.g.* elemental analysis, NMR and IR spectroscopy). One of the simplest ways to overcome this issue is to compare the chromatographic behavior of the ^{99m}Tc complexes with that of the corresponding compounds prepared at the "macroscopic" scale with natural rhenium ("cold metal"), avoiding the use of the long-lived β^--emitter ^{99}Tc for the characterization of the ^{99m}Tc complexes. Despite their differences in terms of ligand exchange reaction kinetics and redox chemistry, Re and Tc present similar physicochemical properties, giving in most of the cases isostructural complexes.

The easy preparation directly from $[MO_4]^-$, the chemical robustness of the *fac*-$[M(CO)_3]^+$ core, and the lability of the three water molecules in *fac*-$[M(CO)_3(H_2O)_3]^+$ (M = Re, Tc) was the driving force toward the design of innovative organometallic probes with unique biological properties. Moreover, the small size

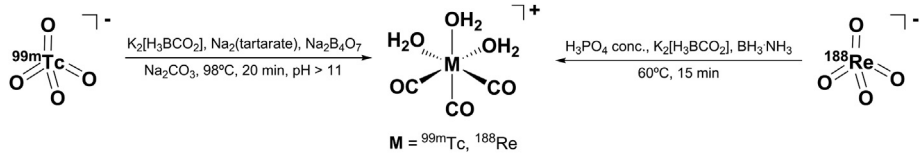

Scheme 1. Aqueous synthesis of *fac*-$[M(CO)_3(H_2O)_3]^+$ (M = ^{99m}Tc, ^{188}Re).

of the metal core allows the labeling of low molecular weight biomolecules with retention of biological activity and specificity [22–31].

The advances in radiopharmaceuticals research, namely in the low oxidation states of ^{99m}Tc, depend strongly on the availability of bifunctional chelators, well-suited to be combined with the various types of biomolecules. Such systems should, preferentially, display high stability, small size, adaptable lipophilicity, absence of isomerism, and easy functionalization [18,32,33]. An ideal BFC would allow the preparation of a radioprobe in high yield, high radiochemical purity, and high specific activity. From a biological point of view, the probe, after intravenous administration, should interact specifically with the respective macromolecular target, and the remaining activity would be rapidly excreted from the non-target organs, preferably by the kidneys, avoiding the hepatobiliary pathway. The final overall biological profile will be influenced by both receptor-specific interactions and "non-specific" mechanisms [18,32,33]. Whereas the factors that influence specific interactions are relatively well understood and can also be studied *in vitro*, those responsible for the non-specific component are less well-defined and depend mainly on the physicochemical features (molecular weight, overall charge and lipophilicity) of the final radiocomplexes. Although the non-specific component of the biodistribution can be predicted, to some extent, *in vitro* (e.g. measuring the protein binding and lipophilicity of the radiotracer), its real assessment can only be done *in vivo* [18,32,33]. In addition, stability is also a key issue regarding pharmacokinetics, since the formation of radioactive metabolites that have lost their targeting capacity may increase significantly the non-specific component of the biodistribution profile.

Taking the above mentioned factors into account, a wide variety of bidentate and tridentate ligands have been evaluated as potential bifunctional chelators for labeling biologically interesting molecules with *fac*-[^{99m}Tc(CO)$_3$]. Owing to our interest in radiopharmaceutical chemistry, namely in the design of innovative target-specific radioactive probes with adequate pharmacokinetic profile for probing molecular targets *in vivo*, we have developed a set of tridentate symmetric and asymmetric pyrazolyl-containing chelators (L) with *N*,*N*,*N* (neutral), *N*,*N*,*O* (monoanionic), *N*,*S*,*O* (monoanionic), *N*,*S*,*N* (neutral), *N*,*S*,*S* (neutral) donor atom sets for stabilization of the core *fac*-[M(CO)$_3$]$^+$ (M = Re, ^{99m}Tc) (Fig. 2) [11,34]. The asymmetric chelators combine in general a pyrazolyl unit with aliphatic amines and/or carboxylic acids or thioethers.

The pyrazolyl-based chelators present a wide range of unique features toward the development of new target-specific probes, namely high stability, water solubility, different coordination possibilities and easy functionalization. These set of features confer a high degree of versatility to the chelators, making them quite suitable for the stabilization of *fac*-[M(CO)$_3$]$^+$ (M = Re, ^{99m}Tc), for conjugation to biomolecules of different nature, and for modulation of the pharmacokinetics of the final complexes. An intrinsic advantage of these systems is their chemical versatility, which allows an easy control of the size and lipophilicity of the complexes, by varying the substituents at the aromatic ring, and different possibilities for biomolecules coupling, with retention of the coordination sphere. Such coupling can be done either at the pyrazolyl ring or at an aliphatic side chain attached to the ligand, through the use of an appropriate functional group (e.g. carboxylic acid). Herein, we will firstly refer briefly to the biological profile of the model ^{99m}Tc(I) complexes stabilized by pyrazolyl-containing chelators. However, the main focus of the present review will be on the use of such type of chelators for labeling relevant biologically active molecules with the organometallic moiety *fac*-[^{99m}Tc(CO)$_3$]$^+$, as well as on the biological assessment of the resulting complexes as SPECT imaging agents in adequate cell and animal models. A special effort will be done to correlate the physicochemical properties of the complexes with their biological properties and potential application.

2. Biological properties of ^{99m}Tc(I) model complexes

Whereas the asymmetric pyrazolyl-containing chelators always coordinate as tridentate, giving well-defined cationic or neutral complexes of the type *fac*-[M(CO)$_3$(k^3-L)]$^{+/0}$ (M = Re, ^{99m}Tc), the coordination behavior of the symmetric chelators depends on the nature of the donor atom set and on the reaction conditions. Therefore, only the asymmetric chelators have been extensively explored toward innovative radiopharmaceutical applications (Fig. 3) [11,34–44].

Among the various asymmetric chelators prepared, **L^1** and **L^2**, which contain the *N*,*N*,*N* donor atom set, allowed the preparation of cationic model complexes of the type *fac*-[M(CO)$_3$(k^3-L)]$^+$ (M = Re, ^{99m}Tc; L = **L^1** and **L^2**) with relevant biological properties (Scheme 2) [35,40,41]. The radioactive complexes *fac*-[^{99m}Tc(CO)$_3$(k^3-L)]$^+$ (L = **L^1** and **L^2**), prepared in high yield, high radiochemical purity, and high specific activity by direct reaction of the respective chelator with the precursor *fac*-[^{99m}Tc(CO)$_3$(H$_2$O)$_3$]$^+$ (Scheme 1), have been characterized by comparing their RP-HPLC traces (γ-detection) with those of the corresponding Re(I) analogs prepared as cold surrogates.

In vitro stability studies have shown that complexes *fac*-[^{99m}Tc(CO)$_3$(k^3-**L^1**)]$^+$ and *fac*-[^{99m}Tc(CO)$_3$(k^3-**L^2**)]$^+$ are more resistant to challenge reactions with biologically relevant amino acid substrates like histidine or cysteine than the related cations anchored by pyrazole-dithioether chelators (*N*,*S*,*S*-donor atom set) [34,36,37]. Biodistribution studies in mice indicated also that these cationic complexes are highly stable *in vivo*, presenting a fast blood clearance and high rate of total radioactivity excretion, occurring primarily through the renal-urinary pathway. The introduction of a carboxylate group in the 4-position of the pyrazolyl ring led to the complexes *fac*-[M(CO)$_3$(k^3-**L^3**)]$^+$ and *fac*-[M(CO)$_3$(k^3-**L^4**)]$^+$, which presented a higher hydrophilic nature and a faster clearance from the main organs than the lead analogs *fac*-[^{99m}Tc(CO)$_3$(k^3-**L^1**)]$^+$ and *fac*-[^{99m}Tc(CO)$_3$(k^3-**L^2**)]$^+$ (Scheme 2) [36,37]. Additionally, the total radioactivity excretion was enhanced, whereas the hepatic retention was reduced. Noteworthy, the presence of the carboxylate group in the heteroaromatic ring of **L^3** and **L^4** enables conjugation to biomolecules, besides modulating the biological profile of the complexes. Considering the stability, variable hydro/lipophilic nature, and biological profile of complexes of the type *fac*-

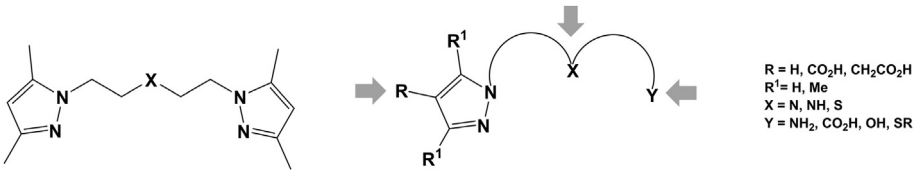

Fig. 2. Tridentate symmetric and asymmetric pyrazolyl-containing chelators (**L**). The potential sites for conjugation to biomolecule are shown for the asymmetric ones.

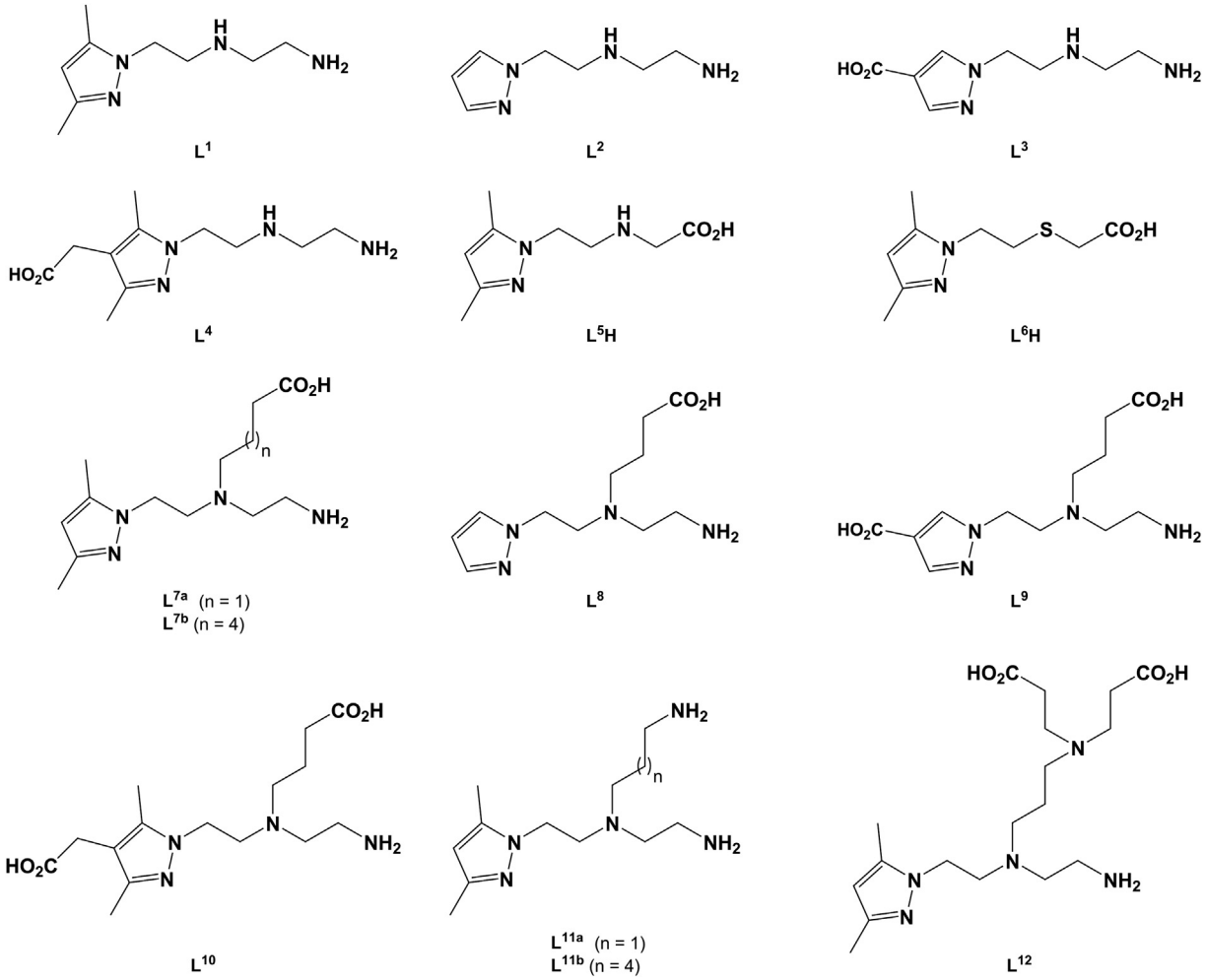

Fig. 3. Asymmetric pyrazolyl-containing chelators [11,34–45].

$[^{99m}Tc(CO)_3(k^3\text{-}\mathbf{L})]^+$, $\mathbf{L^1}$–$\mathbf{L^4}$ appeared as useful chelators for labeling various types of relevant biologically active molecules following a bifunctional approach.

We have also prepared the potentially monoanionic chelators $\mathbf{L^5H}$ (*N*,*N*,*O*-donor atom set) and $\mathbf{L^6H}$ (*N*,*S*,*O*-donor atom set) (Fig. 3), which form neutral complexes of the type *fac*-$[M(CO)_3(k^3\text{-}L)]$ (M = Re, ^{99m}Tc; L = $\mathbf{L^5}$, $\mathbf{L^6}$) by reaction with the appropriate precursor (Scheme 2) [42,43]. The complexes *fac*-$[^{99m}Tc(CO)_3(k^3\text{-}\mathbf{L^5})]$ and *fac*-$[^{99m}Tc(CO)_3(k^3\text{-}\mathbf{L^6})]$ have been characterized by comparing their chromatographic profile with that of the respective Re(I) surrogates, which have been characterized by the usual analytical techniques, including by X-ray crystallography. The chelator $\mathbf{L^5}$ emerged as a promising chelator to be further explored in the design of bifunctional chelators for the labeling of biomolecules with lipophilic character, mainly due to the neutral charge of the corresponding ^{99m}Tc(I) complex.

Based on the lead compounds $\mathbf{L^1}$–$\mathbf{L^4}$, we have also synthesized and characterized the bifunctional chelating analogs $\mathbf{L^{7a/7b}}$, $\mathbf{L^8}$–$\mathbf{L^{10}}$, and $\mathbf{L^{11a/11b}}$, which combine a *N*,*N*,*N* donor atom set for metal coordination and a carboxylate ($\mathbf{L^{7a/7b}}$ and $\mathbf{L^8}$–$\mathbf{L^{10}}$) or amine pendant arm ($\mathbf{L^{11a/11b}}$) at the central amine of the ligand backbone for conjugation to biomolecules (Fig. 3) [36,38,39,44]. These bifunctional chelators react with adequate precursors to afford complexes of the type *fac*-$[M(CO)_3(k^3\text{-}L)]^+$ (M = ^{99m}Tc and Re), in which the chelators act as tridentate through the nitrogen atoms, similarly to what has been observed for the corresponding model complexes (Scheme 2). The ^{99m}Tc complexes were obtained in high yields (≥90%) with high radiochemical purity and specific activity, using ligand concentrations spanning from 10^{-4} to 10^{-5} M. These radioactive complexes are also stable *in vitro* against cysteine and histidine exchange reactions. The biological properties of all ^{99m}Tc(I) complexes stabilized by these bifunctional chelators were assessed in mice at different time points, and compared with those of the corresponding model radioactive complexes previously described. The biodistribution (% I.D./g) and total excretion (%I.D.) for all complexes in CD-1 Charles River mice 4 h after intravenous administration is shown in Table 1.

Analysis of blood and urine samples have shown that complexes are stable *in vivo*, as no radiochemical species follow-on metabolization or transchelation reactions have been detected. Moreover, only a small fraction of the injected radioactivity (≤1.1% I.D./g) was retained in stomach, indicating that none of the complexes underwent *in vivo* re-oxidation to pertechnetate, highlighting again the high stability of the complexes.

The biodistribution data have also shown that all complexes are quite efficiently cleared from blood stream via hepatobiliar and/or renal pathways. None was significantly taken up by any major organ except those involved in the excretory routes like kidneys, liver and intestines. The main differences among them were related to the level of radioactivity retention in these organs, as well as to the percentage of total excretion from whole animal body.

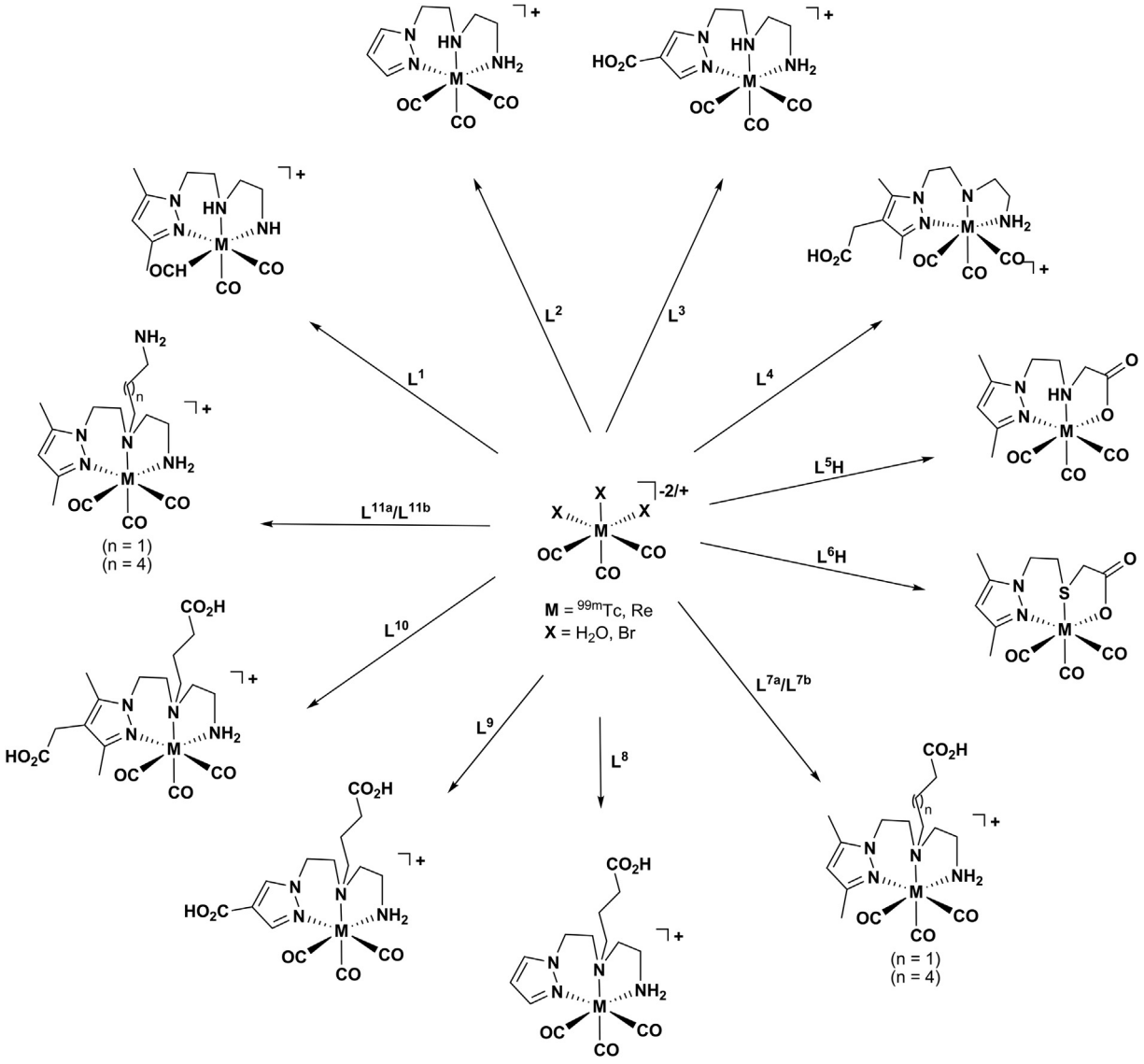

Scheme 2. Synthesis of complexes of the type *fac*-$[M(CO)_3(k^3\text{-}L)]^{+/0}$ stabilized by pyrazolyl-based chelators with *N,X,Y*-donor atom sets (M = Re, ^{99m}Tc; X = N, S; Y = N, O).

The complexes containing pendant carboxylate arms ^{99m}Tc(I)-**L^{7a}**, ^{99m}Tc(I)-**L^{8}**, and ^{99m}Tc(I)-**L^{9}** present considerably lower retention in the excretory pathways and higher percentage of total excretion than those with pendant amine groups (^{99m}Tc(I)-**L^{11a}** and ^{99m}Tc(I)-**L^{11b}**). As expected, the complexes ^{99m}Tc(I)-**L^{7b}** and ^{99m}Tc(I)-**L^{10}**, bearing also carboxylate arms, but with higher molecular weight, present a slower radioactivity excretion rate.

Based on the *in vivo* stability and biological profile of the complexes ^{99m}Tc(I)-**L^{7a}**, ^{99m}Tc(I)-**L^{8}** and ^{99m}Tc(I)-**L^{9}**, the BFCs **L^{7a}**, **L^{8}** and **L^{9}** were considered the most promising for labeling biologically active compounds, being, so far, **L^{7a}** the most explored for that purpose.

Table 1
Biodistribution (% I.D./g) and total excretion (% I.D.) of ^{99m}Tc(CO)$_3$ complexes in CD-1 Charles River mice, 4 h after intravenous administration.

Organ	^{99m}Tc(I)-**L^{7a}**	^{99m}Tc(I)-**L^{7b}**	^{99m}Tc(I)-**L^{8}**	^{99m}Tc(I)-**L^{9}**	^{99m}Tc(I)-**L^{10}**	^{99m}Tc(I)-**L^{11a}**	^{99m}Tc(I)-**L^{11b}**
Blood	0.60 ± 0.10	0.19 ± 0.09	0.15 ± 0.01	0.15 ± 0.02	0.90 ± 0.60	0.13 ± 0.02	0.12 ± 0.01
Liver	2.50 ± 0.20	2.40 ± 0.40	2.72 ± 1.59	0.96 ± 0.27	4.80 ± 1.00	10.80 ± 2.30	16.50 ± 1.80
Intestine	9.90 ± 2.70	15.70 ± 2.40	7.06 ± 0.44	3.35 ± 0.49	13.30 ± 1.90	9.80 ± 1.60	8.00 ± 1,00
Spleen	0.50 ± 0.10	0.34 ± 0.08	0.12 ± 0.01	0.22 ± 0.04	0.38 ± 0.21	0.19 ± 0.06	2.60 ± 0.80
Heart	0.28 ± 0.04	0.06 ± 0.01	0.10 ± 0.01	0.05 ± 0.01	0.37 ± 0.18	0.12 ± 0.01	0.80 ± 0.30
Lung	0.33 ± 0.08	0.15 ± 0.03	0.18 ± 0.01	0.09 ± 0.05	0.45 ± 0.34	0.18 ± 0.06	0.25 ± 0.02
Kidney	1.40 ± 0.20	1.80 ± 0.40	2.34 ± 0.15	0.42 ± 0.05	3.30 ± 0.30	19.80 ± 1.80	46.20 ± 4.60
Muscle	0.10 ± 0.02	0.03 ± 0.01	0.05 ± 0.00	0.02 ± 0.00	0.24 ± 0.04	0.05 ± 0.01	0.11 ± 0.02
Bone	0.12 ± 0.01	0.04 ± 0.02	0.06 ± 0.00	0.03 ± 0.01	0.26 ± 0.04	0.06 ± 0.03	0.13 ± 0.01
Stomach	0.26 ± 0.01	0.20 ± 0.10	0.31 ± 0.12	0.11 ± 0.04	1.00 ± 0.30	1.10 ± 0.20	0.40 ± 0.10
Excretion	60.2 ± 4.8	37.6 ± 5.5	70.7 ± 2.4	85.3 ± 2.0	44.5 ± 2.7	33.9 ± 3.6	25.5 ± 2.9

3. Target-specific ^{99m}Tc(I) complexes

Considering the clinical relevance of different receptor families, intracellular metabolic pathways or endogenous gene expression, we have investigated the possibility of using bioactive peptides, oligonucleotide analogs or low molecular weight compounds, such as enzyme inhibitors/substrates (tyrosine kinase and inducible nitric oxide synthase), for target-specific delivery of *fac*-[^{99m}Tc(CO)$_3$]$^+$ aimed at imaging molecular targets related to various diseases. We have also studied the conjugation of DNA-binding molecules to some of the above described pyrazolyl-diamine chelators, aiming to evaluate the relevance of ^{99m}Tc(I) in the design of Auger-emitting radiopharmaceuticals for targeted therapy. More recently, we have also successfully explored ^{99m}Tc(CO)$_3$-dextran pyrazolyl-diamine derivatives for Sentinel Lymph Node Detection (SLND) at the preclinical level. In the next sections, which are organized according to the nature of the targeting biomolecules, we will present our most relevant achievements in the target-specific delivery of ^{99m}Tc(I) complexes for SPECT-imaging.

3.1. Peptides

During the last years, a significant research effort has been devoted to finding radiolabeled peptides suitable for the *in vivo* detection, functional characterization or therapy of tumors [19–21,46,47]. Such effort has been driven by the favorable features of peptides as carrier molecules that can recognize receptors over-expressed in tumor cells and involved in the different processes underlying tumor pathology, such as proliferation, angiogenesis or metastasis. The most important achievements in this area have been obtained for somatostatin analogs (e.g. ^{111}In-DTPA-octreotide – Octreoscan®), which are clinically relevant for the management of neuroendocrine malignancies [20,21,46,48]. Some progresses have also been reported for other classes of radiolabeled peptides, namely for analogs of bombesin (BBN) or α-melanocyte stimulating hormone (α-MSH), and for peptides containing the ArgGlyAsp amino acid sequence (RGD). We have explored the tricarbonyl technology and pyrazolyl-diamine chelators for ^{99m}Tc-labeling of BBN analogs, cyclic RGD-based peptides and α-MSH analogs, as reviewed herein.

Bombesin (BBN) is a 14 amino acid peptide with very high affinity for the gastrin-releasing peptide receptor (GRPr; BB2 or BBN receptor subtype 2). The GRPr is expressed on a variety of tumors including breast, prostate, pancreatic, and small-cell lung cancer [46,49,50]. Therefore, BBN or BBN derivatives have been used as targeting vectors for the design and development of GRPr-specific diagnostic or therapeutic radiopharmaceuticals [50,51]. BBN conjugates of the type L^{7a}-X-BBN[7–14]NH$_2$ (X = GlyGlyGly, SerSerSer, β-alanine) were synthesized and characterized [36,41]. Competitive binding assays in human prostate PC-3 tumor cells demonstrated specific binding affinity of the L^{7a}-X-BBN[7–14]NH$_2$ conjugates for the GRPr, with IC$_{50}$ values of 0.20 ± 0.02 nM (X = GlyGlyGly), 1.90 ± 0.10 nM (X = SerSerSer) and 0.70 ± 0.04 nM (X = β-alanine). These conjugates allowed the preparation of the radiometallated peptides ^{99m}Tc(CO)$_3$-(L^{7a}-X-BBN[7–14]NH$_2$) (X = GlyGlyGly, SerSerSer, β-alanine) in high radiochemical yield (≥95%) by reaction with the precursor *fac*-[^{99m}Tc(CO)$_3$(H$_2$O)]$^+$ (Fig. 4). All radioactive complexes showed remarkable *in vitro* stability [36,41].

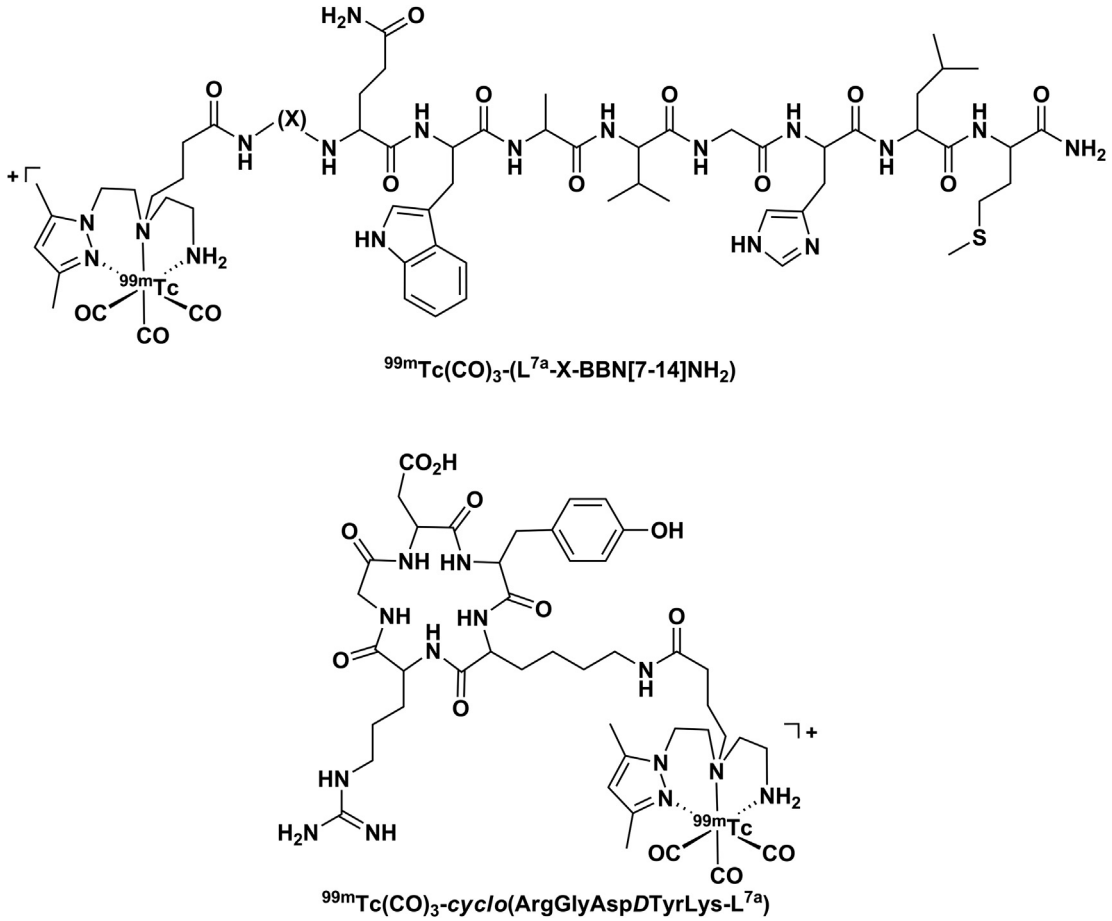

Fig. 4. Radiometallated peptides ^{99m}Tc(CO)$_3$-(L^{7a}-X-BBN[7–14]NH$_2$) (X = GlyGlyGly, SerSerSer, β-alanine) and ^{99m}Tc(CO)$_3$-*cyclo*(ArgGlyAsp*D*TyrLys-L^{7a}).

In vitro internalization and efflux studies in human prostate PC-3 cells showed an agonistic binding behavior for all radiometallated BBN analogs. The highest uptake and residualization of radioactivity was observed for the conjugate containing the β-alanine spacer, however, the exact mechanism for its increased retention is still unclear.

The pharmacokinetic profile of the radiopeptides was evaluated in SCID mice bearing xenografted human prostate PC-3 tumors. A tumor accumulation of 1.76 ± 1.20% ID/g (^{99m}Tc(CO)$_3$(L^{7a}-Gly-GlyGly-BBN[7–14]NH$_2$)), 1.76 ± 0.79% ID/g (^{99m}Tc(CO)$_3$(L^{7a}-Ser-SerSer-BBN[7–14]NH$_2$)), and 1.08 ± 0.41% ID/g (^{99m}Tc(CO)$_3$(L^{7a}-β-alanine-BBN[7–14]NH$_2$)) at 1 h p.i. was found. Blocking studies with "cold" BBN[1–14] reduced the accumulation of radioactivity in the tumor (~22–40% reduction, 1 h pi), demonstrating *in vivo* specificity of these analogs for GRPr-expressing cells.

Radiolabeled peptides containing the RGD amino acid consensus sequence have also been extensively studied to develop site-directed targeting vectors for integrin receptors upregulated on tumor cells and neovasculature [21,52–60]. Integrin recognition of the canonical RGD sequence plays a pivotal role in many cell–cell and cell–extracellular matrix (ECM) interactions. The integrins of most interest in cancer imaging and therapy contain the α_v subunit, particularly the $\alpha_v\beta_3$ and $\alpha_v\beta_5$ subtypes [21,52–60]. Aimed at introducing novel nuclear tools suitable to image angiogenesis and tumor formation *in vivo* by SPECT, the cyclic RGD conjugate *cyclo*-(Arg-Gly-Asp-*D*Tyr-Lys-L^{7a}) has been prepared, and labeled with fac-[^{99m}Tc(CO)$_3$(H$_2$O)]$^+$ to afford the radiopeptide ^{99m}Tc(CO)$_3$-*cyclo*(Arg-Gly-Asp-D-Tyr-Lys-L^{7a}) in high yield (≥90%) and high specific activity (ca. 6 × 10^6 Ci/mol) (Fig. 4) [40].

In vitro internalization and blocking assays in $\alpha_v\beta_3$ receptor-positive human M21 melanoma cancer cells showed that ^{99m}Tc(CO)$_3$-*cyclo*(Arg-Gly-Asp-D-Tyr-Lys-L^{7a}) targets the integrin receptor with high specificity and selectivity. *In vivo* accumulation of radioactivity in mice bearing either $\alpha_v\beta_3$ receptor-positive or negative human melanoma tumors showed receptor specific uptake of the radiotracer with accumulations of 2.50 ± 0.29% ID/g and 0.71 ± 0.08% ID/g in $\alpha_v\beta_3$ integrin positive (M21) and negative (M21L) tumors at 1 h post-injection, respectively. A comparative study with other *cyclo*-RGD peptides labeled with different ^{99m}Tc-cores revealed that ^{99m}Tc(CO)$_3$-*cyclo*(Arg-Gly-Asp-D-Tyr-Lys-L^{7a}) competes well with the best performing compound ([^{99m}Tc]EDDA/HYNIC-RGD) in terms of pharmacokinetic profile and receptor-mediated tumor uptake in mice bearing either $\alpha_v\beta_3$ receptor-positive or negative human melanoma tumors [61].

Melanoma is the most aggressive type of skin cancer due to its high metastatic potential and resistance to current cytotoxic agents. Improvement of patient survival relies mostly on an early diagnosis in combination with an accurate staging of disease extension [62–64]. Therefore, the design of radioactive compounds for melanoma imaging or therapy became a quite attractive approach for the management of both metastatic and non-metastatic melanoma patients [65–67]. Most human and murine melanoma metastasis bear upregulated α-melanocyte stimulating hormone (α-MSH) receptors, namely the melanocortin type 1 receptor (MC1R). α-MSH is the most potent naturally occurring melanotropic peptide and the most active peptide of MC1R (Table 2) [68–71]. In the last few years, a great deal of effort has been directed toward the development of radiolabeled analogs of the tridecapeptide α-MSH for diagnosis (γ- or β$^+$-emitter radionuclides) or treatment (β$^-$-emitter) of melanoma [19,67,72]. Aiming to target the MC1R *in vivo*, we focused our attention on the ^{99m}Tc(CO)$_3$-labeling of linear and cyclic α-MSH analog conjugates bearing a pyrazolyl-diamine chelating unit (Table 2 – Entries 4–11) [11,38,44,72–77].

Table 2
Structure of α-melanocyte-stimulating hormone (α-MSH) and analogs.

Entry	Peptide
1	Ac-Ser-Tyr-Ser- Met^4 -Glu^5-His-Phe-Arg-Trp -Gly-Lys-Pro-Val-NH$_2$ (**α-MSH**)
2	Ac-**Nle**^{4}-**Asp**^{5}-His-***D*Phe**-Arg-Trp-Gly-Lys-NH$_2$ (**NAPamide**)
3	Ac-**Nle**^{4}-**c**[**Asp**^{5}-His-***D*Phe**-Arg-Trp-Lys]-NH$_2$ (**MTII**)
4	**L^{7a}**-βAla^3-**Nle**^{4}-**Asp**^{5}-His-***D*phe**-Arg-Trp-Lys-NH$_2$
5	Ac-**Nle**^{4}-**Asp**^{5}-His-***D*phe**-Arg-Trp-Gly-Lys(**L^{7a}**)-NH$_2$
6	**c**[S–NO$_2$–C$_6$H$_3$–CO–His-***D*phe**-Arg-Trp-Cys]-Lys(**L^{7a}**)–NH$_2$
7	c[NH–NO$_2$–C$_6$H$_3$–CO–His-***D*Phe**-Arg-Trp-Lys]-Lys(**L^{7a}**)–NH$_2$
8	**L^{7a}**-βAla-**Nle-c**[**Asp**-His-***D*Phe**-Arg-Trp-Lys]-NH$_2$
9	**L^8**-βAla-**Nle-c**[**Asp**-His-***D*Phe**-Arg-Trp-Lys]-NH$_2$
10	**L^9**-βAla-**Nle-c**[**Asp**-His-***D*Phe**-Arg-Trp-Lys]-NH$_2$
11	**L^{10}**-βAla-**Nle-c**[**Asp**-His-***D*Phe**-Arg-Trp-Lys]-NH$_2$

We would like to underline that in the case of the cyclic peptide conjugates of the type L-βAla-Nle-c[Asp-His-DPhe-Arg-Trp-Lys]-NH$_2$ (L = **L^{7a}**, **L^8**, **L^9** and **L^{10}**) cyclization involves a lactam bridge through the Lys and Asp side chains [44,74], whereas in the case of c[S–NO$_2$–C$_6$H$_3$–CO–His-*D*Phe-Arg-Trp-Cys]-Lys(L^{7a})–NH$_2$ and c[NH–NO$_2$–C$_6$H$_3$–CO–His-DPhe-Arg-Trp-Lys]-Lys(L^{7a})–NH$_2$, an alkylamine- or alkylthioaryl-bridge [11] is present, respectively.

The peptide conjugates cyclized via a lactam bridge display subnanomolar MC1R binding affinity, as determined in a competition binding assay in B16F1 cells using [^{125}I]-NDP-αMSH as radioligand.

All peptide conjugates react with *fac*-[^{99m}Tc(CO)$_3$(H$_2$O)]$^+$, yielding (>95%) stable radiometallated peptides of the type ^{99m}Tc(CO)$_3$-**L**-α-MSH analog (**L** = **L^{7a}**, **L^8**, **L^9** and **L^{10}**) [11,38,44,72–77].

The cyclic radiopeptides containing a lactam bridge (Fig. 5) present high *in vitro* stability, confirming their resistance to proteolytic degradation caused by endogenous peptidases, and the high ability of the pyrazolyl-diamine chelating unit to stabilize the core *fac*-[^{99m}Tc(CO)$_3$]$^+$, without transmetalation to serum-based proteins or amino acids and/or reoxidation to ^{99m}Tc(VII) [44,74]. Internalization studies in murine B16F1 melanoma cells demonstrated that cellular uptake was MC1R-mediated, suggesting that the affinity of the radiopeptides was preserved upon radiometalation. Indeed, the radiopeptides displayed high level of time-dependent internalization in murine B16F1 melanoma cells, which was strongly inhibited (92–99%) by receptor saturation with NDP-MSH, a known α-MSH analog with high affinity for MC1R (IC$_{50}$ = 0.21 nM) [44,74].

The *in vivo* MC1R-targeting properties of the radiopeptides were evaluated in B16F1 melanoma-bearing mice, and a high melanoma uptake (ca. 10% ID/g) was observed for all radiopeptides at 1 h pi. However, the substitution pattern of the aromatic ring of the chelator had a profound effect on the pharmacokinetic profile of the radiopeptides. The absence of the methyl groups in the azolyl ring of ^{99m}Tc(CO)$_3$-(**L^8**-βAla-Nle-c[Asp-His-DPhe-Arg-Trp-Lys]-NH$_2$) not only reduced significantly the kidney and liver accumulation (87% and 69%, respectively, at 4 h pi) but also increased the total activity excreted by urinary route (51%, at 4 h pi) when compared with ^{99m}Tc(CO)$_3$-(**L^{7a}**-βAla-Nle-c[Asp-His-DPhe-Arg-Trp-Lys]-NH$_2$). Nevertheless, a considerable accumulation of ^{99m}Tc(CO)$_3$-(**L^8**-βAla-Nle-c[Asp-His-DPhe-Arg-Trp-Lys]-NH$_2$) in the liver and kidney (4.02 ± 0.17 and 7.09 ± 0.42% ID/g, respectively) was observed at 4 h pi. The radiopeptides ^{99m}Tc(CO)$_3$-(**L^9**-βAla-Nle-c[Asp-His-DPhe-Arg-Trp-Lys]-NH$_2$) and ^{99m}Tc(CO)$_3$-(**L^{10}**-βAla-Nle-c[Asp-His-DPhe-Arg-Trp-Lys]-NH$_2$) presented a striking kidney and liver uptake reduction (>90%, at 4 h pi) upon comparison with [^{99m}Tc(CO)$_3$-(**L^{7a}**-βAla-**Nle-c**[**Asp**-His-***D*Phe**-Arg-Trp-Lys]-NH$_2$)]. Moreover, the overall radioactivity elimination of both radiopeptides occurred mainly through the renal pathway, and the

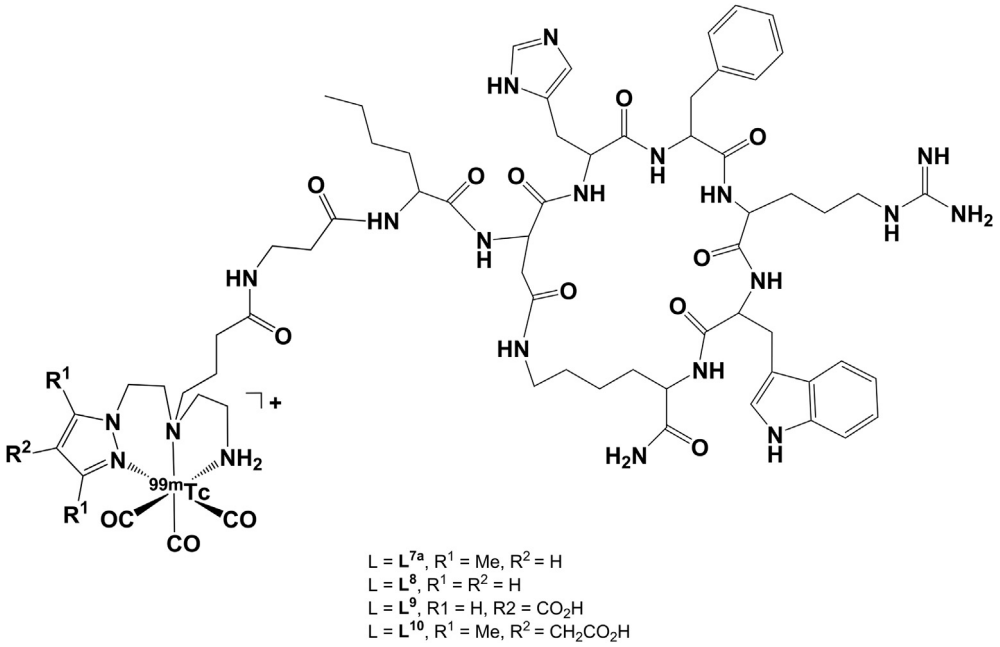

Fig. 5. Structure of the lactam-based cyclic $^{99m}Tc(CO)_3$-labeled α-MSH analogs of the type **L**-βAla-Nle-c[Asp-His-DPhe-Arg-Trp-Lys]-NH_2 (**L** = $\mathbf{L^{7a}}$, $\mathbf{L^{8}}$, $\mathbf{L^{9}}$ and $\mathbf{L^{10}}$).

whole body clearance was faster than that observed for $^{99m}Tc(CO)_3$-($\mathbf{L^{7a}}$-βAla-Nle-c[Asp-His-DPhe-Arg-Trp-Lys]-NH_2). The favorable biodistribution profile of $^{99m}Tc(CO)_3$-($\mathbf{L^{9}}$-βAla-Nle-c[Asp-His-DPhe-Arg-Trp-Lys]-NH_2)] and $^{99m}Tc(CO)_3$-($\mathbf{L^{10}}$-βAla-Nle-c[Asp-His-DPhe-Arg-Trp-Lys]-NH_2) allows a clear visualization of flank melanoma lesions in tumor-bearing mice by SPECT-imaging at 1 h pi. Moreover, an enhanced tumor-to-kidney and tumor-to-liver ratios for both compounds generated high contrast between tumor and background. As an illustrative example, Fig. 6 presents planar scintigraphic images of B16F1 murine melanoma-bearing C57BL/6 mice injected with $^{99m}Tc(CO)_3$-($\mathbf{L^{9}}$-βAla-Nle-c[Asp-His-DPhe-Arg-Trp-Lys]-NH_2) at 1 h pi.

In addition to their high potential as melanoma imaging agents demonstrated at the preclinical level, the results presented herein highlight how the selection of the most appropriate ligand for an organometallic compound may tune/modulate its biological properties. Indeed, this study demonstrated that structural modifications on the chelating system, particularly the introduction of carboxylate groups shifts the excretion pathway of a radiopeptide from mainly hepatobiliar toward mainly renal and, simultaneously, improves notably tumor-to-non-target-organs ratios.

With the aim of applying the multivalency concept to melanoma imaging, we have designed homobivalent conjugates ([NAPamide]$_2$-**L**, L = $\mathbf{L^{12}}$, $\mathbf{L^{10}}$) containing a pyrazolyl-diamine chelating unit and two copies of the targeting peptide NAPamide (Table 2, Entry 1), a linear α-MSH analog. The two peptide units are separated by linkers of different nature ($\mathbf{L^{12}}$, symmetric alkyl chain; $\mathbf{L^{10}}$, asymmetric semi-rigid spacer) and length ($\mathbf{L^{12}}$, 9 atoms; $\mathbf{L^{10}}$, 14 atoms) [38]. The *in vitro* MC1R-binding affinity of the bivalent conjugates was found to be 19-fold ($\mathbf{L^{12}}$) and 4-fold ($\mathbf{L^{10}}$) higher than that of the monovalent NAPamide conjugate ($\mathbf{L^{7a}}$), previously described [75]. Metalation of the bivalent conjugates yielded isostructural complexes of the type *fac*-[$M(CO)_3$([NAPamide]$_2$-**L**)], with the rhenium complexes *fac*-[$Re(CO)_3$([NAPamide]$_2$-$\mathbf{L^{12}}$)] and *fac*-[$Re(CO)_3$([NAPamide]$_2$-$\mathbf{L^{10}}$)] displaying binding affinities in the subnanomolar and nanomolar range (Fig. 7).

Cell internalization studies in B16F1 murine melanoma cells have shown that *fac*-[$^{99m}Tc(CO)_3$([NAPamide]$_2$-$\mathbf{L^{10}}$)] and *fac*-

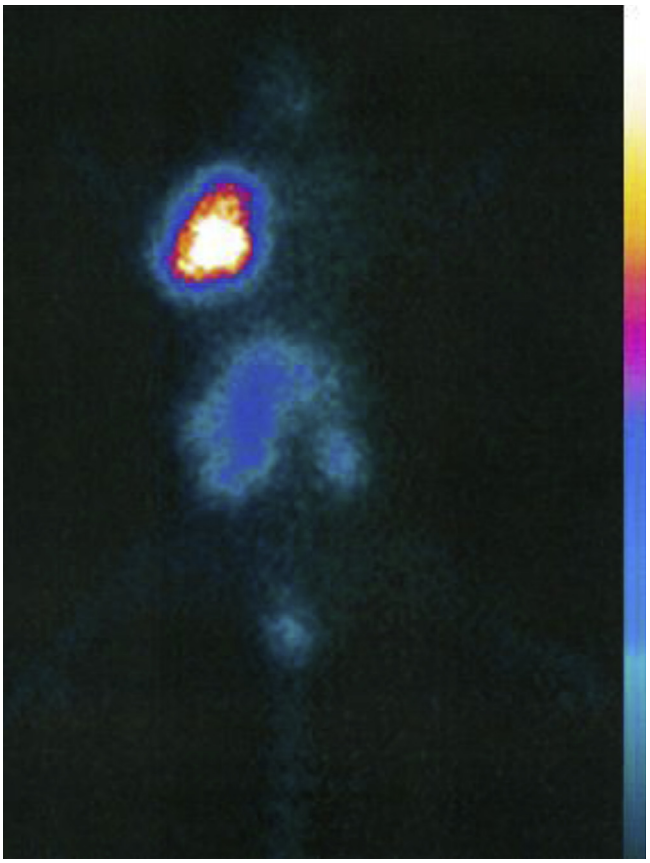

Fig. 6. Planar scintigraphic image of B16F1 murine melanoma-bearing C57BL/6 mice injected with $^{99m}Tc(CO)_3$-($\mathbf{L^{9}}$-βAla-Nle-c[Asp-His-DPhe-Arg-Trp-Lys]-NH_2) at 1 h p.i. [44]. Adapted with permission from M. Morais, B.L. Oliveira, J.D.G. Correia, M.C. Oliveira, M.A. Jimenez, I. Santos, P.D. Raposinho, Influence of the bifunctional chelator on the pharmacokinetic properties of $^{99m}Tc(CO)_3$-labeled cyclic alpha-melanocyte stimulating hormone analog, J. Med. Chem. 56 (2013) 1961–1973. Copyright 2013 American Chemical Society.

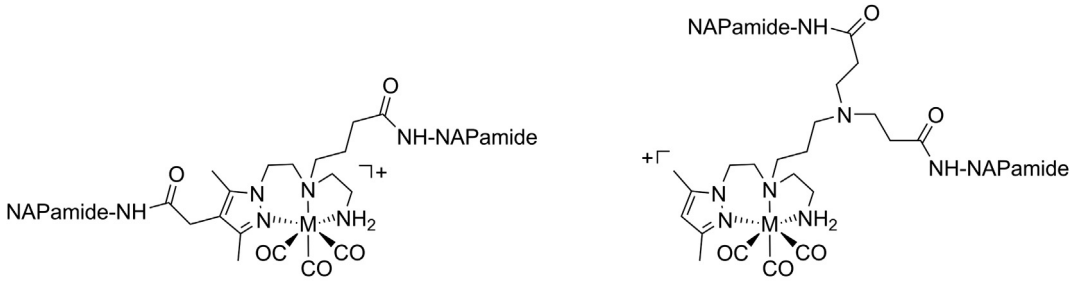

Fig. 7. Metalated homobivalent α-MSH analogs (M = ^{99m}Tc, Re).

[^{99m}Tc(CO)$_3$([NAPamide]$_2$-**L^{12}**)] internalize via an MC1R-mediated mechanism. The biodistribution studies in B16F1 melanoma bearing mice have shown that melanoma uptake correlates well with the *in vitro* MC1R binding affinity of the rhenium surrogates (*fac*-[Re(CO)$_3$([NAPamide]$_2$-**L^{12}**)], IC$_{50}$ = 0.15 nM; *fac*-[Re(CO)$_3$([NAPamide]$_2$-**L^{10}**)], IC$_{50}$ = 1.14 nM). However, there is no positive correlation between tumor uptake and valency, even in the case of *fac*-[^{99m}Tc(CO)$_3$([NAPamide]$_2$-**L^{12}**)], which had the highest cellular internalization level and better retention.

3.2. Peptide nucleic acids

Peptide nucleic acids (PNAs) are DNA analogs in which the sugar–phosphate backbone has been replaced by a pseudopeptide chain constituted by *N*-(2-aminoethyl)glycine [78–82]. PNAs are achiral, neutral, and stable over a wide range of pH, resistant to enzymatic degradation, and do not activate RNase H degradation of mRNA. They can also bind to complementary DNA/RNA, resulting in hybrid PNA/DNA or PNA/RNA duplexes, which are thermodynamically more stable than the homoduplexes [78–82]. PNAs and their derivatives have been used as potential drugs, or as components for designing radioactive probes for *in vivo* imaging of endogenous gene expression trough the antisense strategy [83,84]. The latter approach is directed to transcription of genes into messenger RNA (mRNA), using a complementary sequence of the target mRNA for imaging.

With the goal of exploring the possibility of labeling clinically relevant PNA sequences with the organometallic core *fac*-[^{99m}Tc(CO)$_3$]$^+$ we have synthesized and characterized the 16-mer peptide nucleic acid sequence H-AGAT CAT GCC CGG CAT-Lys-NH$_2$, complementary to the translation start region of the *N*-myc oncogene messenger RNA [85–88], and coupled it to **L^{7a}**, yielding the novel PNA-conjugate **L^{7a}**-A GAT CAT GCC CGG CAT-Lys-NH$_2$ [89,90]. The conjugate was labeled with *fac*-[^{99m}Tc(CO)$_3$]$^+$, affording quantitatively *fac*-[^{99m}Tc(CO)$_3$(**L^{7a}**-A GAT CAT GCC CGG CAT-Lys-NH$_2$)]$^{2+}$ in high specific activity. The identity of the radiocomplex was confirmed by comparing its HPLC profile with that of the rhenium surrogate. UV melting experiments of H-AGAT CAT GCC CGG CAT-Lys-NH$_2$ and *fac*-[Re(CO)$_3$(**L^{7a}**-A GAT CAT GCC CGG CAT-Lys-NH$_2$)]$^{2+}$ with the complementary DNA sequence, led to the formation of stable duplexes, indicating that the conjugation of the 16-mer peptide nucleic acid sequence to the bifunctional chelator and to the metal fragment *fac*-[M(CO)$_3$]$^+$ did not affect the recognition of the complementary sequence and the duplex stability.

Cell internalization and retention studies in *N*-myc expressing SH-SY5Y human neuroblastoma cells, have shown that *fac*-[^{99m}Tc(CO)$_3$-**L^{7a}**-A GAT CAT GCC CGG CAT-Lys-NH$_2$)]$^{2+}$ internalizes with a relatively high cellular retention (only 40% of internalized activity is released from the cells after 5 h). These values are in line with the reported higher permeability of neuronal cell lines to PNA, and with the internalization of a rhodamine-conjugated PNA into neuroblastoma cells.

3.3. Dextran-based polymeric nanoparticles for sentinel lymph node detection

Most recently, we have described the first class of fully characterized ^{99m}Tc(CO)$_3$-mannosylated dextran derivatives with relevant biological properties for sentinel lymph node detection (SLND) [91,92]. Dextran derivatives, containing the same number of pendant mannose units (13) and a variable number (*n*) of pyrazolyl-diamine chelating units for ^{99m}Tc(CO)$_3$ labeling (*n* = 1, 4 and 8), have been synthesized and fully characterized. Radiolabeled polymers have been obtained quantitatively in high radiochemical purity (98%) upon reaction of the dextran derivatives with *fac*-[^{99m}Tc(CO)$_3$(H$_2$O)$_3$]$^+$ [91]. The radioactive species were identified by comparing their γ-traces in the HPLC chromatograms with the UV/Vis traces of the corresponding rhenium surrogates, which have been characterized both at the chemical (NMR and IR spectroscopy, and HPLC) and physical level (Dynamic Light Scattering, Atomic Force Microscopy and Laser Doppler Velocimetry). SPECT-CT imaging and biodistribution studies in Wistar rats with one of the radioactive polymers (13 mannose units, 8 pyrazolyl-diamine units) have shown good accumulation in the sentinel node at 60 min post injection, with significant retention up to 180 min [93]. A clear delineation of the SLN without significant washout to other regions was observed in the scintigraphic images (Fig. 8). These findings demonstrate that ^{99m}Tc(CO)$_3$-labeled dextran polymeric

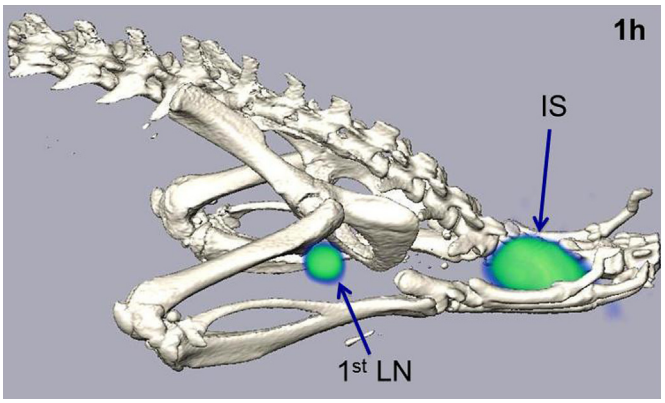

Fig. 8. SPECT-CT image of a Wistar rat after subcutaneous injection of a ^{99m}Tc(CO)$_3$-mannosylated dextran derivative at 1 h p.i., with clear delineation of the sentinel lymph node [93]. IS = Injection site, 1st LN = sentinel lymph node.

nanoparticles are promising and merit further evaluation as radiopharmaceuticals for SLND at the clinical set.

3.4. Small biomolecules

3.4.1. Estradiol derivatives

With the aim of imaging ER-positive breast tumors by SPECT, we have explored the possibility of using ^{99m}Tc(CO)$_3$-labeled estradiol derivatives containing a pyrazolyl-diamine chelating unit, based on **L^1**, for targeting the estrogen receptor (ER). However, preliminary ER binding affinity assays and cellular internalization studies in an ER expressing cell line, MCF-7, suggested a non ER mediated uptake mechanism [94,95].

3.4.2. L-Arg derivatives

Nitric Oxide Synthase (NOS) is the enzyme responsible for the catalytic oxidation of L-arginine (L-Arg) to L-citrulline and nitric oxide (NO), an endogenous free radical, which is a key signaling mammalian mediator in several pathophysiological processes [96]. NOS is a heme-containing protein that presents two constitutively expressed isoforms (neuronal NOS, nNOS and endothelial NOS, eNOS) and one inducible isoform (iNOS). The isoforms differ in their tissue distribution and biological role [97]. The low levels of NO resulting from the activity of the constitutive isoforms regulate blood pressure, platelet aggregation and neurotransmission. The iNOS is expressed and induced at a transcriptional level by inflammatory stimuli (e.g. interferon, IFN-γ and bacterial lipopolysaccharide), and the relatively high levels of NO produced by this isoform are linked to several diseases, including stroke, hypertension, cancer, and rheumatoid arthritis, among others [98–100]. Thus, the *in vivo* imaging of NO/NOS expression would allow earlier diagnosis, earlier treatment, better prognosis and individualized patient management of the diseases associated to NO/NOS deregulation [101]. Considering our interest in the design of innovative radiometal-based complexes as probes for *in vivo* molecular imaging of NOS, a set of M(CO)$_3$-complexes (M = ^{99m}Tc, Re) containing pendant NOS-recognizing units have been designed [39,102,103]. Among the various Re(CO)$_3$-complexes prepared as "cold" surrogates of the analog ^{99m}Tc(CO)$_3$-complexes, those containing a pendant N$^{\omega}$-NO$_2$-L-Arg moiety with known inhibitory ability toward NOS, displayed the most favorable targeting properties. In contrast, the complexes bearing a pendant L-Arg moiety substrate of NOS, lost completely the ability to recognize the enzyme. The complexes containing chelators with a propyl *fac*-[Re(CO)$_3$(**L^{7a}**-Prop-N$^{\omega}$-NO$_2$-L-Arg)] or an hexyl spacer *fac*-[Re(CO)$_3$(**L^{7b}**-Hex-N$^{\omega}$-NO$_2$-L-Arg)], in which the α-NH$_2$ group of N$^{\omega}$-NO$_2$-L-Arg is involved in the conjugation to the metal center, presented remarkable affinity for purified iNOS, being similar to that of the free non-conjugated inhibitor (K_i = 3–8 μM) in the case of the complex bearing the hexyl spacer (K_i = 6 μM) (Fig. 9).

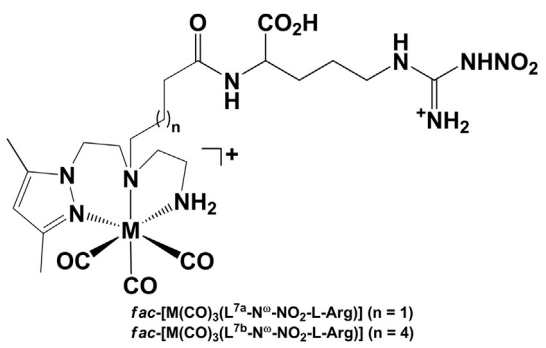

Fig. 9. ^{99m}Tc/Re tricarbonyl complexes with a pendant N$^{\omega}$-NO$_2$-L-Arg moiety.

Interestingly, the rhenium complexes presented higher inhibitory potency than the respective metal-free conjugates. Additionally, these complexes permeate through RAW 264.7 macrophage cell membranes, interacting specifically with the target enzyme in the cytosol, as confirmed by the suppression of NO biosynthesis (30%–50%) in Lipopolysaccharide(LPS)-treated macrophages. The respective ^{99m}Tc(CO)$_3$ analog complexes also presented the ability to cross cell membranes, as demonstrated by internalization studies in the same cell model. Preliminary biodistribution studies in LPS-pretreated mature female C57BL6 mice suggest that the complexes accumulate in tissues with iNOS upregulation. With the goal of establishing a preliminary structure–activity relationship, we performed a molecular docking study to evaluate the binding modes of the N$^{\omega}$-NO$_2$-L-Arg-containing conjugates and of the corresponding rhenium complexes [15,104,105]. Molecular dynamics simulations were used to refine the conformations obtained by docking and to identify the most prevalent interactions between the Re complexes and the iNOS isoform, more specifically, between the "Re(CO)$_3$" metallic fragment and the active site of the enzyme. The higher inhibitory effect of the rhenium compound with the hexyl spacer (*fac*-[Re(CO)$_3$(L^{7b}-Hex-N$^{\omega}$-NO$_2$-L-Arg)]) arises from the stronger, unique, electrostatic interactions observed between the "Re(CO)$_3$" core and the residues Arg-260 and Arg-382 (Fig. 10). This interaction, is only possible due to the higher flexibility associated to the C6-carbon linker when compared to the C3 linker present in the other rhenium analog. Moreover, the computational studies demonstrated that the metal center plays a key role in the organization and orientation of the organic ligands, defining the overall shape of the inhibitors that fit better in the active pocket of iNOS.

In conclusion, computational methods may be useful for predicting the affinity of putative novel rhenium and technetium complexes. Such an approach may provide strategies for the design of novel metal-based substrates/inhibitors with unique shapes and higher structural diversity with the aim of targeting NOS *in vivo* more effectively.

3.4.3. Quinazoline derivatives

Tumor imaging of EGFR receptors with radioactive probes has been a field of intense research in the last years, namely based on tyrosine kinase inhibitors such as quinazoline derivatives [108–116]. The radiolabeling of small molecule protein kinase inhibitors for imaging protein kinase expression by PET or SPECT has been recently reviewed, highlighting the importance of the topic in the development of novel target specific agents for imaging cancer or the central nervous system [117]. Searching for useful ^{99m}Tc(I) probes for early detection and staging of EGFR positive tumors, we have conjugated the quinazoline pharmacophore (3-chloro-4-fluorophenyl)quinazoline-4,6-diamine (TKi) to a bifunctional chelator based on **L^{5}H** (Fig. 3), which contains a *N*,*N*,*O*-donor atom set [42,118]. The corresponding complex *fac*-[^{99m}Tc(CO)$_3$(**L^5**-TKi)] was obtained in quantitative yield and with high radiochemical purity after optimization of the labeling conditions to avoid cleavage of the pendant arm carrying the pharmacophore (Fig. 11). *In vitro* studies confirmed that the corresponding rhenium surrogate *fac*-[Re(CO)$_3$(**L^5**-TKi)] still inhibits significantly the EGFR autophosphorylation and also inhibited A431 cell growth.

3.4.4. Bisphosphonates

The drawbacks associated to the ^{99m}Tc-labeled bisphosphonates (^{99m}Tc-BP) routinely used for bone imaging (^{99m}Tc-MDP, MDP = methylenediphosphonate, and ^{99m}Tc-HMDP, HMDP = hydroxymethylenediphosphonate), namely *in vivo* instability, and relatively slow blood and soft-tissue clearance [119–123], prompted us to design novel ^{99m}Tc(CO)$_3$-based bone-seeking radiotracers

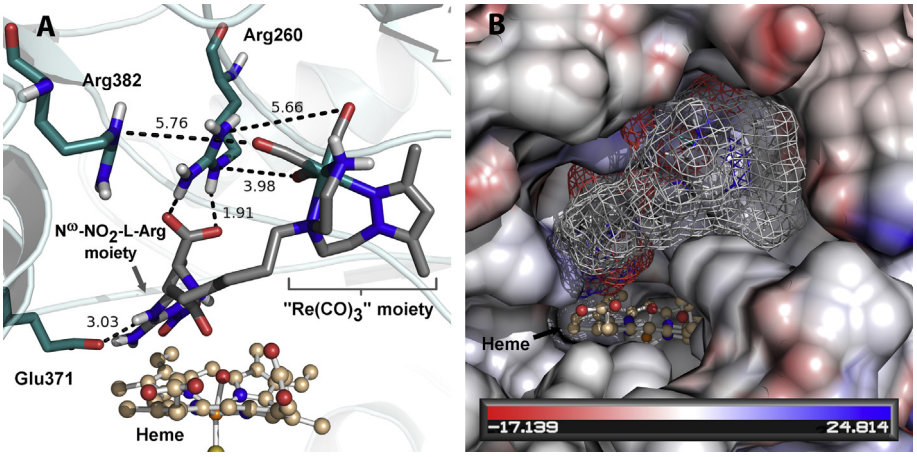

Fig. 10. **A**: Proposed structure of *fac*-[Re(CO)$_3$(L^{7b}-N$^{\omega}$-NO$_2$-L-Arg)] in complex with iNOS obtained by MD simulation [15,104]. The following color scheme is used: nitrogen in blue, oxygen in red, sulfur in yellow, iron in orange and rhenium in deep teal. All distances shown in Å. **B**: Molecular surface of the active site of the same system colored according to electrostatic potential. The Figure was generated using the VASCo PyMOL plug-in [106,107]. (For interpretation of the references to color in this figure legend, the reader is referred to the web version of this article.)

with improved chemical and biological properties [124–128]. Among the various phosphonate-containing radioactive complexes prepared, the well-defined stable complexes *fac*-[^{99m}Tc(CO)$_3$(**L^{7a}**-PAM)]$^-$ and *fac*-[^{99m}Tc(CO)$_3$(**L^{7a}**-ALN)]$^-$, which comprise the bifunctional chelator **L^{7a}** for metal stabilization and a pendant pamidronate (PAM) or alendronate (ALN) moiety for bone targeting, have emerged as the most promising for bone targeting (Fig. 11) [128]. The biodistribution studies in Balb-c mice demonstrated that both radiotracers presented high bone uptake (ca. 18% I.D./g, at 1 h post injection), similar to the gold standard ^{99m}Tc-MDP, with comparable clearance from most tissues and increased total excretion. The bone-to-blood and the bone-to-muscle ratios are higher than the ones found for ^{99m}Tc-MDP at 4 h post injection.

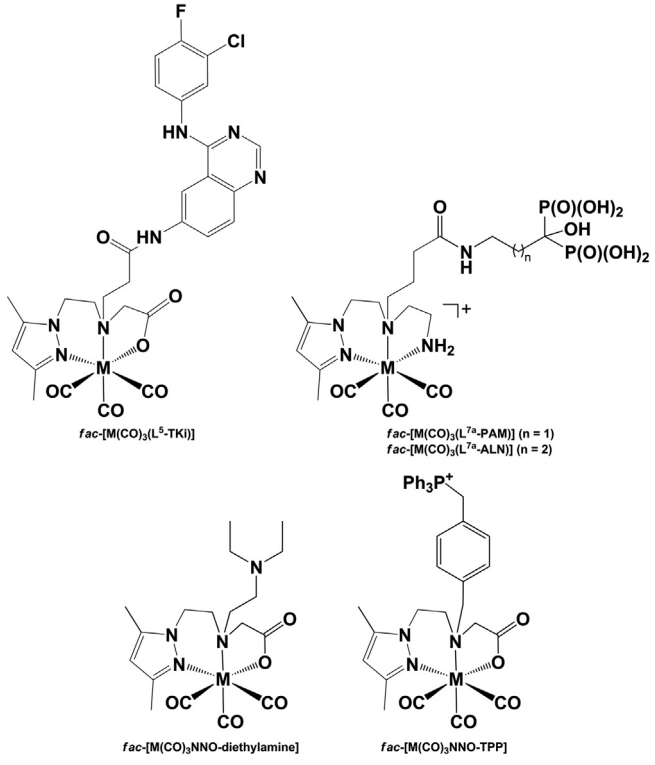

Fig. 11. Metal tricarbonyl complexes (M = ^{99m}Tc, Re) bearing pendant small molecules.

Planar whole-body gamma camera images of Sprague Dawley rats injected with *fac*-[^{99m}Tc(CO)$_3$(**L^{7a}**-PAM)]$^-$ and *fac*-[^{99m}Tc(CO)$_3$(**L^{7a}**-ALN)]$^-$ confirmed the overall adequate biological profile of the new radiotracers for bone imaging. As an illustrative example, a whole body image of a Sprague Dawley rat acquired at 2 h after injection of *fac*-[^{99m}Tc(CO)$_3$(pz-ALN)]$^-$ is presented in Fig. 12.

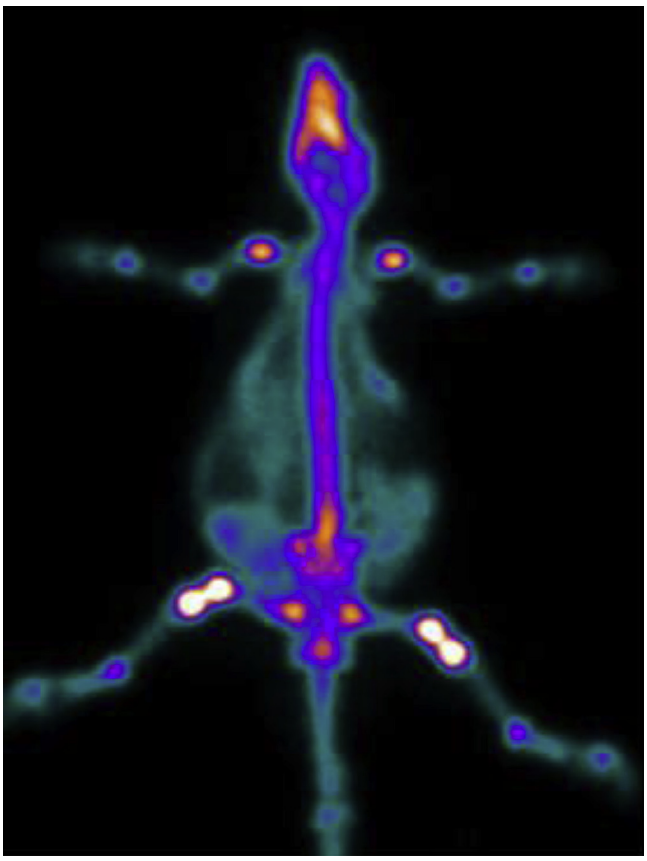

Fig. 12. Planar whole-body gamma camera image of a rat injected with *fac*-[^{99m}Tc(CO)$_3$(**L^{7a}**-ALN)]$^-$, 2 h p.i. [128]. E. Palma, J.D.G. Correia, B.L. Oliveira, L. Gano, I.C. Santos, I. Santos, ^{99m}Tc(CO)$_3$-labeled pamidronate and alendronate for bone imaging, Dalton Trans. 40 (2011) 2787–2796. Reproduced by permission of The Royal Society of Chemistry.

3.4.5. Benzamide and triphenylphosphonium (TPP) derivatives

Benzamide derivatives are a class of small organic molecules with relevance for *in vivo* targeting of melanoma and its metastases. As already mentioned, early diagnosis of melanoma and accurate follow-up can decrease mortality and provide the best chance for optimal clinical management. Previously, encouraging results have been reported for radioiodinated benzamides, which in some cases have undergone clinical trials [129]. We have studied a large family of neutral and cationic $^{99m}Tc(CO)_3$-complexes with pyrazolyl-based tridentate N_3- and N_2O-donor ligands bearing benzamides or their fragments as melanin binders, as exemplified for [$^{99m}Tc(CO)_3$(NNO-diethylamine)] in Fig. 11. In general, these complexes displayed moderate to high *in vitro* affinity for synthetic melanin [130–132]. Some of them showed a moderate tumor uptake in a B16-F1 melanoma-bearing mouse and rather favorable target/non-target ratios.

Triphenylphosphonium (TPP) derivatives are another class of small organic molecules that has been explored in the design of target-specific radiopharmaceuticals due to their well known ability to accumulate in the energized mitochondria of tumor cells [133–135]. We have investigated TPP-containing Re/^{99m}Tc organometallic compounds as probes for *in vivo* targeting of energized mitochondria, using bifunctional chelators of the pyrazole-diamine (*N*,*N*,*N*-donor atom set) and pyrazole-aminocarboxylic (*N*,*N*,*O*-donor atom set) type [136]. The synthesized complexes presented a dicationic or monocationic character and their lipophilicity was readily tuned by the use of different spacers (butylene *vs p*-xylene) to link the TPP pharmacophore to the central amine of the corresponding tridentate chelators. *In vitro* studies have shown that these complexes accumulate in different types of tumor cells, being the mitochondria a relevant intracellular target as pointed out by the results obtained with isolated mitochondria. For the complex with the highest mitochondrial uptake, *fac*-[$^{99m}Tc(CO)_3$NNO-TPP] (Fig. 11), the *in vitro* studies suggested the accumulation in mitochondria of tumor cells by diffusion, in favor of the electrochemical gradient and showing a strong dependency on the mitochondrial and plasma membrane potentials. Moreover, this complex has shown a higher affinity toward tumor mitochondria than toward normal mitochondria, as well as a higher uptake in human tumor cells if compared with normal cells from human origin. Altogether, these results indicate that TPP-containing $^{99m}Tc(I)$ tricarbonyl complexes are promising platforms to design radioactive metalloprobes targeted to the mitochondria for *in vivo* detection of tumor tissues.

3.5. DNA-binders

^{99m}Tc-complexes may hold potential for targeted antitumor therapy since ^{99m}Tc is also an Auger-electron emitting radiometal. However, due to the short range of Auger electrons, there is a need for preferential accumulation of the complexes into the nucleus of the tumor cells in order to elicit significant DNA damage, and consequently a therapeutic effect [137,138]. Therefore, the improvement of the therapeutic efficiency of ^{99m}Tc requires the design of compounds having a better ability to target the nucleus. This type of study was pioneered by Alberto and co-workers, who have shown that a trifunctional $^{99m}Tc(I)$ tricarbonyl complex, containing a pyrene intercalator and a NLS peptide, can reach the nucleus of B16-F1 mouse melanoma cells and induce much stronger radiotoxic effects than [$^{99m}TcO_4$]$^-$.The same group has observed that related tricarbonyl $^{99m}Tc(I)$ or Re(I) complexes bearing acridine orange as a DNA-binding group could also target the nucleus of murine B16F1 cells without the presence of a carrier NLS sequence [139]. With the goal of developing $^{99m}Tc(I)$ radiopharmaceuticals for targeted radiotherapy, and taking advantage of the versatile nature of pyrazolyl-diamine chelators, we have evaluated $^{99m}Tc(I)$/Re(I) tricarbonyl complexes bearing anthracene ([$^{99m}Tc(CO)_3$(**L^1**-Anthr)]$^+$) or acridine orange ([$^{99m}Tc(CO)_3$(**L^4**-AO)]$^+$) groups for DNA interaction (Fig. 13) [140–143]. Both complexes rapidly entered the cells and accumulate in the nucleus. Complex [$^{99m}Tc(CO)_3$(**L^1**-Anthr)]$^+$ exhibited pronounced radiotoxic effects and induced an apoptotic cellular outcome [141].

Complex [$^{99m}Tc(CO)_3$(**L^4**-AO)]$^+$ was further "decorated" with a pendant bombesin (BBN) analog (GlyGlyGlyBBN[7–14]) for receptor-mediated uptake in cells overexpressing the gastrin releasing peptide receptor (GRPr) [144]. The resulting complex $^{99m}Tc(CO)_3$(**L^{10}**-AO-GlyGlyGlyBBN[7–14]) presented high and specific cellular internalization in PC3 cells and a remarkably high nuclear uptake in the same cell line. Live cell confocal imaging microscopy studies with the Re surrogate complex have shown a considerable accumulation of fluorescence into the nucleus with uptake kinetics similar to that exhibited by [$^{99m}Tc(CO)_3$(**L^4**-AO)]$^+$

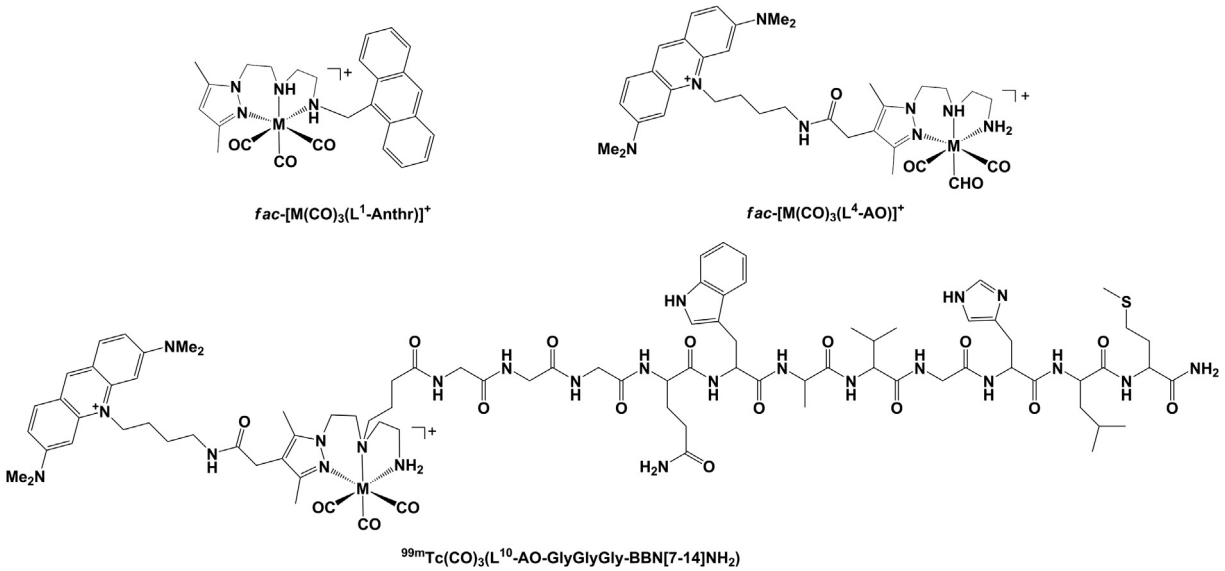

Fig. 13. M(I) tricarbonyl complexes functionalized with polyaromatic DNA intercalators (M = ^{99m}Tc, Re).

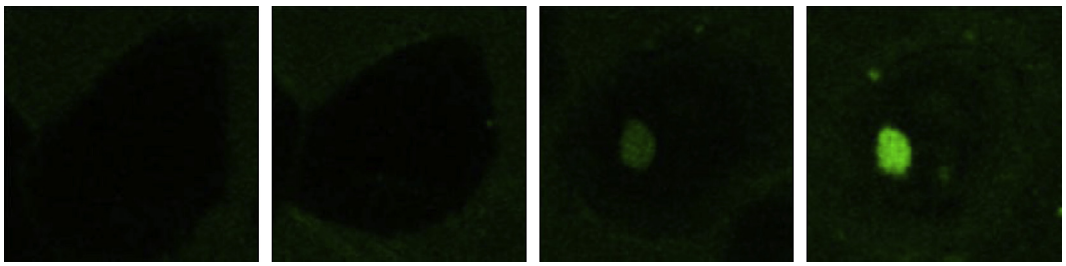

Fig. 14. Live cell uptake of complex $Re(CO)_3(\mathbf{L^{10}}$-AO-GlyGlyGlyBBN[7–14]) in PC3 cells, visualized by time-lapse confocal microscopy imaging [144].

(Fig. 14). These compounds are the first examples of multifunctional ^{99m}Tc(I) bioconjugates that combine specific cell targeting with nuclear internalization, a crucial issue for the exploitation of ^{99m}Tc in Auger therapy.

4. Conclusions

The tridentate asymmetric pyrazolyl-containing chelators with *N*,*N*,*N* (neutral) or *N*,*N*,*O* (monoanionic) donor atom sets reviewed herein have several favorable features (e.g. high stability, water solubility, easy functionalization and coordination possibilities) for the design of innovative ^{99m}Tc(I)-based target-specific probes. Such versatility led to the preparation of a wide variety of well-defined cationic or neutral complexes of the type *fac*-$[M(CO)_3(k^3\text{-}L)]^{+/0}$ (M = Re, ^{99m}Tc) in high yield. The ^{99m}Tc(I) model complexes were stable against cysteine and histidine exchange reactions and toward oxidation. The high stability, together with the adequate biological profile, indicated that the chelators could be further explored in the design of bifunctional chelating ligands for the labeling of biomolecules. Our studies revealed that the functionalization of the model chelators through the central secondary amine, as well as through the pyrazolyl ring, did not change the coordination ability of the bifunctional chelators toward the tricarbonyl unit, and did not affect the *in vivo* stability of the resulting complexes. Taking advantage of such properties, tumor-seeking peptides (bombesin and α-MSH analogs, and peptides containing the RGD sequence) and a peptide nucleic acid (PNA) have been conjugated to the chelators and labeled in high yield and high specific activity with the moiety *fac*-$[^{99m}Tc(CO)_3]^+$. Despite exhibiting promising tumor-targeting properties, the pharmacokinetic profile of some of the labeled peptides has still to be further improved. Besides peptides, low molecular weight biomolecules such as quinazoline derivatives, bisphosphonates, L-arginine derivatives, benzamides, TPP derivatives and DNA binders have also been labeled in high yield and high specific activity with retention of biological activity, as assessed using appropriate cell and animal models. In addition, we have also labeled polymeric nanoparticles based on dextran for sentinel lymph node detection (SLND), which allowed the visualization of the SLN accurately at the preclinical level. In conclusion, the versatility of the pyrazolyl-containing chelators allowed the preparation of ^{99m}Tc(I) complexes with tunable physicochemical and biological properties for the labeling of a wide range of relevant biomolecules, spanning from small organic pharmacophores to dextran-based polymeric nanoparticles.

Acknowledgments

Fundação para a Ciência e Tecnologia (FCT) is acknowledged for financial support (projects PTDC/QUI-QUI/121752/2010 and PTDC/QUI-QUI/115712/2009). M. Morais thanks FCT for a PhD grant (SFRH/BD/48066/2008). Support of the IAEA is acknowledged trough the Coordinated Research Project on the "Development of ^{99m}Tc radiopharmaceuticals for sentinel node detection and cancer diagnosis".

References

[1] G.P. Saha, Fundamentals of Nuclear Pharmacy, sixth ed., Springer, New York, 2010.
[2] S. Vallabhajosula, L. Solnes, B. Vallabhajosula, Seminars in Nuclear Medicine 41 (2011) 246–264.
[3] S.L. Pimlott, A. Sutherland, Chemical Society Reviews 40 (2011) 149–162.
[4] T.J. Wadas, E.H. Wong, G.R. Weisman, C.J. Anderson, Chemical Reviews 110 (2010) 2858–2902.
[5] M.D. Bartholoma, A.S. Louie, J.F. Valliant, J. Zubieta, Chemical Reviews 110 (2010) 2903–2920.
[6] I. Velikyan, Theranostics 2 (2012) 424–426.
[7] F. Tisato, M. Porchia, C. Bolzati, F. Refosco, A. Vittadini, Coordination Chemistry Reviews 250 (2006) 2034–2045.
[8] G. Bandoli, F. Tisato, A. Dolmella, S. Agostini, Coordination Chemistry Reviews 250 (2006) 561–573.
[9] R. Garcia, A. Paulo, I. Santos, Inorganica Chimica Acta 362 (2009) 4315–4327.
[10] A. Boschi, A. Duatti, L. Uccelli, Contrast Agents III: Radiopharmaceuticals – From Diagnostics to Therapeutics 252 (2005) 85–115.
[11] G.R. Morais, A. Paulo, I. Santos, Organometallics 31 (2012) 5693–5714.
[12] S. Liu, Advanced Drug Delivery Reviews 60 (2008) 1347–1370.
[13] S. Liu, Contrast Agents III: Radiopharmaceuticals – From Diagnostics to Therapeutics 252 (2005) 117–153.
[14] F. Mendes, A. Paulo, I. Santos, Dalton Transactions 40 (2011) 5377–5393.
[15] A. Almeida, B.L. Oliveira, J.D.G. Correia, G. Soveral, A. Casini, Coordination Chemistry Reviews (2013).
[16] R. Weissleder, M.J. Pittet, Nature 452 (2008) 580–589.
[17] M. Schwaiger, A. Beer, S. Ziegler, H.J. Wester, European Journal of Cancer 48 (2012) S13–S14.
[18] H.J. Wester, Clinical Cancer Research 13 (2007) 3470–3481.
[19] J.D.G. Correia, A. Paulo, P.D. Raposinho, I. Santos, Dalton Transactions 40 (2011) 6144–6167.
[20] M. Fani, H.R. Maecke, S.M. Okarvi, Theranostics 2 (2012) 481–501.
[21] M. Fani, H.R. Maecke, European Journal of Nuclear Medicine and Molecular Imaging 39 (Suppl. 1) (2012) S11–S30.
[22] R. Alberto, Medicinal Organometallic Chemistry 32 (2010) 219–246.
[23] R. Alberto, European Journal of Inorganic Chemistry (2009) 21–31.
[24] R. Alberto, Journal of Organometallic Chemistry 692 (2007) 1179–1186.
[25] R. Alberto, Chimia 61 (2007), 691–691.
[26] U. Abram, R. Alberto, Journal of the Brazilian Chemical Society 17 (2006) 1486–1500.
[27] R. Alberto, Contrast Agents III: Radiopharmaceuticals – From Diagnostics to Therapeutics 252 (2005) 1–44.
[28] R. Alberto, J.K. Pak, D. van Staveren, S. Mundwiler, P. Benny, Biopolymers 76 (2004) 324–333.
[29] R. Alberto, European Journal of Nuclear Medicine and Molecular Imaging 30 (2003) 1299–1302.
[30] R. Schibli, R. Schwarzbach, R. Alberto, K. Ortner, H. Schmalle, C. Dumas, et al., Bioconjugate Chemistry 13 (2002) 750–756.
[31] R. Alberto, K. Ortner, N. Wheatley, R. Schibli, A.P. Schubiger, Journal of the American Chemical Society 123 (2001) 3135–3136.
[32] S.J. Mather, Molecular Biosystems 3 (2007) 30–35.
[33] C. Decristoforo, S.J. Mather, Quarterly Journal of Nuclear Medicine 46 (2002) 195–205.
[34] I. Santos, A. Paulo, J.D.G. Correia, Current Radiopharmaceuticals 2 (2009) 277–294.
[35] S. Alves, A. Paulo, J.D.G. Correia, A. Domingos, I. Santos, Journal of the Chemical Society, Dalton Transactions (2002) 4714–4719.
[36] S. Alves, A. Paulo, J.D.G. Correia, L. Gano, C.J. Smith, T.J. Hoffman, et al., Bioconjugate Chemistry 16 (2005) 438–449.
[37] R.F. Vitor, S. Alves, J.D.G. Correia, A. Paulo, I. Santos, Journal of Organometallic Chemistry 689 (2004) 4764–4774.
[38] M.M. Morais, P.D. Raposinho, J.D.G. Correia, I. Santos, Journal of Peptide Science 16 (2010), 186–186.

[39] B.L. Oliveira, P.D. Raposinho, F. Mendes, F. Figueira, I. Santos, A. Ferreira, et al., Bioconjugate Chemistry 21 (2010) 2168–2172.
[40] S. Alves, J.D.G. Correia, L. Gano, T.L. Rold, A. Prasanphanich, R. Haubner, et al., Bioconjugate Chemistry 18 (2007) 530–537.
[41] S. Alves, J.D.G. Correia, I. Santos, B. Veerendra, G.L. Sieckman, T.J. Hoffman, et al., Nuclear Medicine and Biology 33 (2006) 625–634.
[42] C. Fernandes, I.C. Santos, I. Santos, H.J. Pietzsch, J.U. Kunstler, W. Kraus, et al., Dalton Transactions (2008) 3215–3225.
[43] C. Moura, C. Fernandes, L. Gano, A. Paulo, I.C. Santos, I. Santos, et al., Journal of Organometallic Chemistry 694 (2009) 950–958.
[44] M. Morais, B.L. Oliveira, J.D. Correia, M.C. Oliveira, M.A. Jimenez, I. Santos, et al., Journal of Medicinal Chemistry 56 (2013) 1961–1973.
[45] M. Videira, F. Silva, A. Paulo, I.C. Santos, I. Santos, Inorganica Chimica Acta 362 (2009) 2807–2813.
[46] J.C. Reubi, H.R. Maecke, Journal of Nuclear Medicine 49 (2008) 1735–1738.
[47] M. Schottelius, H.J. Wester, Methods 48 (2009) 161–177.
[48] D. Wild, M. Fani, M. Behe, I. Brink, J.E. Rivier, J.C. Reubi, et al., Journal of Nuclear Medicine 52 (2011) 1412–1417.
[49] J.C. Reubi, Endocrine Reviews 24 (2003) 389–427.
[50] C.J. Smith, W.A. Volkert, T.J. Hoffman, Nuclear Medicine and Biology 32 (2005) 733–740.
[51] V. Sancho, A. Di Florio, T.W. Moody, R.T. Jensen, Current Drug Delivery 8 (2011) 79–134.
[52] R.H. Haubner, H.J. Wester, W.A. Weber, M. Schwaiger, Quarterly Journal of Nuclear Medicine 47 (2003) 189–199.
[53] R. Haubner, H.J. Wester, Current Pharmaceutical Design 10 (2004) 1439–1455.
[54] R. Haubner, W.A. Weber, A.J. Beer, E. Vabuliene, D. Reim, M. Sarbia, et al., PLOS Medicine 2 (2005) e70.
[55] R. Haubner, European Journal of Nuclear Medicine and Molecular Imaging 33 (Suppl. 1) (2006) 54–63.
[56] A.J. Beer, A.L. Grosu, J. Carlsen, A. Kolk, M. Sarbia, I. Stangier, et al., Clinical Cancer Research 13 (2007) 6610–6616.
[57] R. Haubner, Handbook of Experimental Pharmacology (2008) 323–339.
[58] R. Haubner, C. Decristoforo, Frontiers in Bioscience 14 (2009) 872–886.
[59] R. Haubner, A.J. Beer, H. Wang, X. Chen, European Journal of Nuclear Medicine and Molecular Imaging 37 (Suppl. 1) (2010) S86–S103.
[60] U. Tateishi, T. Oka, T. Inoue, Current Medicinal Chemistry 19 (2012) 3301–3309.
[61] C. Decristoforo, I. Santos, H.J. Pietzsch, J.U. Kuenstler, A. Duatti, C.J. Smith, et al., The Quarterly Journal of Nuclear Medicine and Molecular Imaging 51 (2007) 33–41.
[62] V. Gray-Schopfer, C. Wellbrock, R. Marais, Nature 445 (2007) 851–857.
[63] J.A. Carlson, A. Slominski, G.P. Linette, M.C. Mihm, J.S. Ross, Expert Review of Molecular Diagnostics 3 (2003) 303–330.
[64] J.A. Carlson, A. Slominski, G.P. Linette, M.C. Mihm, J.S. Ross, Expert Review of Molecular Diagnostics 3 (2003) 163–184.
[65] Y.B. Miao, T.P. Quinn, Critical Reviews in Oncology Hematology 67 (2008) 213–228.
[66] G. Ren, Y. Pan, Z. Cheng, Current Pharmaceutical Biotechnology 11 (2010) 590–602.
[67] T. Quinn, X. Zhang, Y. Miao, Giornale Italiano Di Dermatologia E Venereologia 145 (2010) 245–258.
[68] G.E. Ghanem, G. Comunale, A. Libert, A. Vercammengrandjean, F.J. Lejeune, International Journal of Cancer 41 (1988) 248–255.
[69] W. Siegrist, F. Solca, S. Stutz, L. Giuffre, S. Carrel, J. Girard, et al., Cancer Research 49 (1989) 6352–6358.
[70] F. Solca, W. Siegrist, R. Drozdz, J. Girard, A.N. Eberle, Journal of Biological Chemistry 264 (1989) 14277–14281.
[71] W. Siegrist, S. Stutz, A.N. Eberle, Cancer Research 54 (1994) 2604–2610.
[72] P.D. Raposinho, J.D.G. Correia, M.C. Oliveira, I. Santos, Biopolymers 94 (2010) 820–829.
[73] M. Valldosera, M. Monso, C. Xavier, P. Raposinho, J.D.G. Correia, I. Santos, et al., International Journal of Peptide Research and Therapeutics 14 (2008) 273–281.
[74] P.D. Raposinho, C. Xavier, J.D.G. Correia, S. Falcao, P. Gomes, I. Santos, Journal of Biological Inorganic Chemistry 13 (2008) 449–459.
[75] P.D. Raposinho, J.D.G. Correia, S. Alves, M.F. Botelho, A.C. Santos, I. Santos, Nuclear Medicine and Biology 35 (2008) 91–99.
[76] M. Morais, P.D. Raposinho, M.C. Oliveira, J.D.G. Correia, I. Santos, Biopolymers 96 (2011), 515–515.
[77] M. Morais, P.D. Raposinho, M.C. Oliveira, J.D.G. Correia, I. Santos, Journal of Biological Inorganic Chemistry 17 (2012) 491–505.
[78] V.A. Kumar, European Journal of Organic Chemistry (2002) 2021–2032.
[79] S. Basu, E. Wickstrom, Bioconjugate Chemistry 8 (1997) 481–488.
[80] V. Menchise, G. De Simone, T. Tedeschi, R. Corradini, S. Sforza, R. Marchelli, et al., Proceedings of the National Academy of Sciences of the United States of America 100 (2003) 12021–12026.
[81] H. Rasmussen, J. Sandholm, Nature Structural Biology 4 (1997) 98–101.
[82] A. Ray, B. Norden, FASEB Journal 14 (2000) 1041–1060.
[83] D.J. Hnatowich, K. Nakamura, Annals of Nuclear Medicine 18 (2004) 363–368.
[84] X.K. Sun, H.F. Fang, X.X. Li, R. Rossin, M.J. Welch, J.S. Taylor, Bioconjugate Chemistry 16 (2005) 294–305.
[85] R. Tonelli, S. Purgato, C. Camerin, R. Fronza, F. Bologna, S. Alboresi, et al., Molecular Cancer Therapeutics 4 (2005) 779–786.
[86] N. Watanabe, H. Sawai, I. Ogihara-Umeda, S. Tanada, E.E. Kim, Y. Yonekura, et al., Journal of Nuclear Medicine 47 (2006) 1670–1677.
[87] A. Pession, R. Tonelli, R. Fronza, E. Sciamanna, R. Corradini, S. Sforza, et al., International Journal of Oncology 24 (2004) 265–272.
[88] R. Howman-Giles, P.J. Shaw, R.F. Uren, D.K.V. Chung, Seminars in Nuclear Medicine 37 (2007) 286–302.
[89] C. Xavier, J.K. Pak, I. Santos, R. Alberto, Journal of Organometallic Chemistry 692 (2007) 1332–1339.
[90] C. Xavier, C. Giannini, L. Gano, S. Maiorana, R. Alberto, I. Santos, Journal of Biological Inorganic Chemistry 13 (2008) 1335–1344.
[91] M. Morais, S. Subramanian, U. Pandey, G. Samuel, M. Venkatesh, M. Martins, et al., Molecular Pharmaceutics 8 (2011) 609–620.
[92] I. Pirmettis, Y. Arano, T. Tsotakos, K. Okada, A. Yamaguchi, T. Uehara, et al., Molecular Pharmaceutics 9 (2012) 1681–1692.
[93] Y. Arano, A. Yamaguchi, T. Uehara, M. Morais, J.D.G. Correia, I. Santos, 2013, unpublished results.
[94] C. Neto, M.C. Oliveira, L. Gano, F. Marques, I. Santos, T. Thiemann, Nuclear Medicine and Biology 37 (2010) 699–700.
[95] C. Neto, M.C. Oliveira, L. Gano, F. Marques, T. Thiemann, I. Santos, Journal of Inorganic Biochemistry 111 (2012) 1–9.
[96] J.F. Kerwin, J.R. Lancaster, P.L. Feldman, Journal of Medicinal Chemistry 38 (1995) 4343–4362.
[97] S. Moncada, R.M.J. Palmer, E.A. Higgs, Pharmacological Reviews 43 (1991) 109–142.
[98] R. Korhonen, A. Lahti, H. Kankaanranta, E. Moilanen, Current Drug Targets – Inflammation & Allergy 4 (2005) 471–479.
[99] D. Fukumura, S. Kashiwagi, R.K. Jain, Nature Reviews Cancer 6 (2006) 521–534.
[100] A.J. Duncan, S.J. Heales, Molecular Aspects of Medicine 26 (2005) 67–96.
[101] H. Hong, J. Sun, W. Cai, Multimodality imaging of nitric oxide and nitric oxide syntheses, Free Radical Biology & Medicine 47 (2009) 684–698.
[102] B.L. Oliveira, J.D. Correia, P.D. Raposinho, I. Santos, A. Ferreira, C. Cordeiro, et al., Dalton Transactions (2009) 152–162.
[103] B.L. Oliveira, P.D. Raposinho, F. Mendes, I.C. Santos, I. Santos, A. Ferreira, et al., Journal of Organometallic Chemistry 696 (2011) 1057–1065.
[104] B.L. Oliveira, I.S. Moreira, P.A. Fernandes, M.J. Ramos, I. Santos, J.D.G. Correia, unpublished results, 2012.
[105] B.L. Oliveira, I.S. Moreira, P.A. Fernandes, M.J. Ramos, I. Santos, J.D. Correia, Journal of Molecular Modeling 19 (2013) 1537–1551.
[106] G. Steinkellner, R. Rader, G.G. Thallinger, C. Kratky, K. Gruber, BMC Bioinformatics (2009) 10.
[107] W.L. DeLano, The PyMOL Molecular Graphics System, DeLano Scientific, San Carlos, CA, USA, 2002.
[108] J.J. Laskin, A.B. Sandler, Cancer Treatment Reviews 30 (2004) 1–17.
[109] R. Bianco, T. Gelardi, V. Damiano, F. Ciardiello, G. Tortora, The International Journal of Biochemistry & Cell Biology 39 (2007) 1416–1431.
[110] R. Zandi, A.B. Larsen, P. Andersen, M.T. Stockhausen, H.S. Poulsen, Cell Signal 19 (2007) 2013–2023.
[111] C. Arteaga, Seminars in Oncology 30 (2003) 3–14.
[112] R.D. Mass, International Journal of Radiation Oncology Biology Physics 58 (2004) 932–940.
[113] J. Albanell, P. Gascon, Current Drug Targets 6 (2005) 259–274.
[114] A.P. Pintado, S.J. Mather, M.A. Stalteri, D. Allison, A.P. Capote, A.H. Cairo, et al., Journal of Radioanalytical and Nuclear Chemistry 275 (2008) 619–626.
[115] G. Abourbeh, S. Dissoki, O. Jacobson, A. Litchi, R. Ben Daniel, D. Laki, et al., Nuclear Medicine and Biology 34 (2007) 55–70.
[116] M. Shaul, G. Abourbeh, O. Jacobson, Y. Rozen, D. Laky, A. Levitzki, et al., Bioorganic & Medicinal Chemistry 12 (2004) 3421–3429.
[117] J.W. Hicks, H.F. VanBrocklin, A.A. Wilson, S. Houle, N. Vasdev, Molecules 15 (2010) 8260–8278.
[118] N. Margaritis, A. Bourkoula, A. Chiotellis, M. Papadopoulos, A. Panagiotopoulou, C. Tsoukalas, et al., A New Technetium-99m Biomarker for EGFR-TK, SGE Editoriali, Padova, 2006, pp. 523–524.
[119] C. Love, A.S. Din, M.B. Tomas, T.P. Kalapparambath, C.J. Palestro, Radiographics 23 (2003) 341–358.
[120] S.F. Zhang, G. Gangal, H. Uludag, Chemical Society Reviews 36 (2007) 507–531.
[121] K. Verbeke, J. Rozenski, B. Cleynhens, H. Vanbilloen, T. de Groot, N. Weyns, et al., Bioconjugate Chemistry 13 (2002) 16–22.
[122] J. Doubsky, M. Laznicek, A. Laznickova, L. Leseticky, Journal of Radioanalytical and Nuclear Chemistry 260 (2004) 53–59.
[123] J. Liu, F.L. Wang, J.B. Zhang, S.Y. Yang, H.X. Guo, X.B. Wang, Journal of Labelled Compounds & Radiopharmaceuticals 50 (2007) 1243–1247.
[124] E. Palma, J.D.G. Correia, M.P.C. Campello, I. Santos, Molecular Biosystems 7 (2011) 2950–2966.
[125] E. Palma, B.L. Oliveira, F. Figueira, J.D.G. Correia, P.D. Raposinho, I. Santos, Journal of Labelled Compounds & Radiopharmaceuticals 50 (2007) 1176–1184.
[126] E. Palma, B.L. Oliveira, J.D. Correia, L. Gano, L. Maria, I.C. Santos, et al., Journal of Biological Inorganic Chemistry 12 (2007) 667–679.
[127] E. Palma, J.D.G. Correia, L. Gano, I. Santos, Nuclear Medicine and Biology 37 (2010), 711–711.
[128] E. Palma, J.D.G. Correia, B.L. Oliveira, L. Gano, I.C. Santos, I. Santos, Dalton Transactions 40 (2011) 2787–2796.
[129] A. Maisonial, B. Kuhnast, J. Papon, R. Boisgard, M. Bayle, A. Vidal, et al., Journal of Medicinal Chemistry 54 (2011) 2745–2766.

[130] C. Moura, L. Gano, F. Mendes, P.D. Raposinho, A.M. Abrantes, M.F. Botelho, et al., European Journal of Medicinal Chemistry 50 (2012) 350–360.
[131] C. Moura, T. Esteves, L. Gano, P.D. Raposinho, A. Paulo, I. Santos, New Journal of Chemistry 34 (2010) 2564–2578.
[132] C. Moura, L. Gano, P.D. Raposinho, I.C. Santos, A. Paulo, I. Santos, Nuclear Medicine and Biology 37 (2010), 703–703.
[133] M.L. Vallano, M. Sonenberg, Journal of Membrane Biology 68 (1982) 57–66.
[134] I. Madar, L. Weiss, G. Izbicki, Journal of Nuclear Medicine 43 (2002) 234–238.
[135] D. Lichtstein, H.R. Kaback, A.J. Blume, Proceedings of the National Academy of Sciences of the United States of America 76 (1979) 650–654.
[136] C. Moura, F. Mendes, L. Gano, I. Santos, A. Paulo, Journal of Inorganic Biochemistry 123C (2013) 34–45.
[137] A.I. Kassis, Journal of Nuclear Medicine 44 (2003) 1479–1481.
[138] M. Ginj, K. Hinni, S. Tschumi, S. Schulz, H.R. Maecke, Journal of Nuclear Medicine 46 (2005) 2097–2103.
[139] P. Haefliger, N. Agorastos, A. Renard, G. Giambonini-Brugnoli, C. Marty, R. Alberto, Bioconjugate Chemistry 16 (2005) 582–587.
[140] R.F. Vitor, I. Correia, M. Videira, F. Marques, A. Paulo, J.C. Pessoa, et al., ChemBioChem 9 (2008) 131–142.
[141] R.F. Vitor, T. Esteves, F. Marques, P. Raposinho, A. Paulo, S. Rodrigues, et al., Cancer Biotherapy and Radiopharmaceuticals 24 (2009) 551–563.
[142] T. Esteves, F. Marques, J. Rino, A. Paulo, C.J. Smith, I. Santos, Nuclear Medicine and Biology 37 (2010), 710–710.
[143] F. Marques, A. Paulo, M.P. Campello, S. Lacerda, R.F. Vitor, L. Gano, et al., Radiation Protection Dosimetry 116 (2005) 601–604.
[144] T. Esteves, F. Marques, A. Paulo, J. Rino, P. Nanda, C.J. Smith, et al., Journal of Biological Inorganic Chemistry 16 (2011) 1141–1153.